*Chapter in* **Advancing Astrophysics with the SKA – II**

# Synergies for the Epoch of Reionization and Cosmic Dawn

Anirban Chakraborty,[1] Tirthankar R. Choudhury,[1] Kanan K. Datta,[2] Pratika Dayal,[3,4,5] Jiten Dhandha,[6,7] Samuel Gagnon-Hartman,[8] Sambit K. Giri,[9,10] Adélie Gorce,[11] Caroline Heneka,[12] Anne Hutter,[13] Barun Maity,[14] Suman Majumdar,[15] Andrei Mesinger,[16] Kana Moriwaki,[17,18] Chandra Shekhar Murmu,[19] Yuxiang Qin,[20] Shintaro Yoshiura[21] and Erik Zackrisson[22]

[1]*National Centre for Radio Astrophysics, Tata Institute of Fundamental Research, Pune 411007, India*
[2]*Relativity & Cosmology Research Centre, Department of Physics, Jadavpur University, Kolkata 700032, India*
[3]*Canadian Institute for Theoretical Astrophysics, 60 St George St, University of Toronto, Toronto, ON M5S 3H8, Canada*
[4]*David A. Dunlap Department of Astronomy and Astrophysics, University of Toronto, 50 St George St, Toronto ON M5S 3H4, Canada*
[5]*Department of Physics, 60 St George St, University of Toronto, Toronto, ON M5S 3H8, Canada*
[6]*Institute of Astronomy, University of Cambridge, Madingley Road, Cambridge CB30HA, United Kingdom*
[7]*Kavli Institute for Cosmology, Madingley Road, Cambridge CB30HA, United Kingdom*
[8]*Scuola Normale Superiore di Pisa, Piazza dei Cavallieri 7, 56126 Pisa, Italy*
[9]*Department of Astronomy and Oskar Klein Centre, AlbaNova, Stockholm University, SE-10691 Stockholm, Sweden*
[10]*Van Swinderen Institute for Particle Physics and Gravity, University of Groningen, Nijenborgh 3, 9747 AG Groningen, The Netherlands*
[11]*Université Paris-Saclay, CNRS, Institut d'Astrophysique Spatiale, 91405, Orsay, France*
[12]*Institut für Theoretische Physik, Universität Heidelberg, Philosophenweg 16, 69120 Heidelberg, Germany*
[13]*Institute for Astronomy, University of Vienna, Türkenschanzstrasse 17, A-1180 Vienna, Austria*
[14]*Max-Planck-Institut für Astronomie, Königstuhl 17, D-69117 Heidelberg, Germany*
[15]*Department of Astronomy, Astrophysics & Space Engineering, Indian Institute of Technology Indore, Indore 453552, India*
[16]*Department of Physics and Astronomy "Ettore Majorana", University of Catania, Via Santa Sofia 64, 95123 Catania, Italy*
[17]*Research Center for the Early Universe, Graduate School of Science, The University of Tokyo, 7-3-1 Hongo, Bunkyo, Tokyo 113-0033, Japan*
[18]*Department of Physics, Graduate School of Science, The University of Tokyo, 7-3-1 Hongo, Bunkyo, Tokyo 133-0033, Japan*
[19]*Astrophysics Research Centre of the Open University (ARCO) & Department of Natural Sciences, The Open University of Israel, 1 University Road, POBox808, Ra'anana 4353701, Israel*
[20]*Research School of Astronomy and Astrophysics, Australian National University, Canberra, ACT 2611, Australia*
[21]*Mizusawa VLBI Observatory, National Astronomical Observatory of Japan, 2-21-1 Osawa, Mitaka, Tokyo 181-8588, Japan*

 

[22]*Observational Astrophysics, Department of Physics and Astronomy, Uppsala University, Box 516, SE-751 20 Uppsala, Sweden*

E-mail: andrei.mesinger@dfa.unict.it

Synergies with other instruments will be *essential* in making, verifying, and interpreting a detection of the cosmic 21-cm signal from the Epoch of Reionization (EoR) and Cosmic Dawn (CD) with the SKA-low telescope. Such synergies can (i) provide prior information about galaxies and the intergalactic medium (IGM) during the EoR/CD; (ii) pave the road to a first 21cm detection by mitigating foregrounds and systematics through cross-correlations; and (iii) give complimentary physical insights into the galaxy – IGM connection. Here we review the current state of synergies and discuss what observations will best compliment SKA-low EoR/CD observations.

## 1 Introduction

The Epoch of Reionization (EoR) remains one of the central frontiers of modern cosmology. After decades of research, we are beginning to constrain the timing of the main phase of reionization (e.g. Planck Collaboration et al. 2016; Greig et al. 2017; Mason et al. 2018; Bosman et al. 2022; Qin et al. 2025). Yet, we still lack a clear understanding of how to connect this cosmic milestone to the populations of stars and black holes that powered it.

The most powerful probe of this era is the 21-cm line from neutral hydrogen, which traces fluctuations in ionization, temperature, and density of the intergalactic medium (IGM). Current interferometers aim to detect the 21-cm power spectrum statistically (e.g. Paciga et al. 2011; Acharya et al. 2024; Yoshiura et al. 2021; HERA Collaboration et al. 2023). SKA-Low in Australia promisses to deliver the first 3D tomographic map of the early Universe, providing unprecedented insights into the astrophysics of galaxies, the IGM, and cosmology itself (e.g. Mesinger 2020).

However, high–signal-to-noise (S/N) 21-cm maps of the EoR and the preceding Cosmic Dawn (CD) are still years away. Initial detections will likely involve only a few low-S/N power-spectrum modes. Given the novelty of the observation, confirming that such signals are truly cosmological will be challenging. The most robust way to validate them—and to enhance S/N—is through cross-correlation with independent tracers of known cosmic origin.

Cross-correlations not only provide a sanity check on early detections but also yield cleaner cosmological signals, since foregrounds and instrumental systematics in different datasets are typically uncorrelated. Moreover, multi-wavelength observations of the same volume provide complementary insights into the physics governing the galaxy – IGM connection during the EoR. Eventually, with an expanded SKA (Phase 2), it will be possible to correlate full 3D images from different probes, enabling detailed studies of individual ionized or heated regions—comparing their 21-cm morphology with the brightest galaxies they host, as observed by *JWST* and future optical/IR facilities.

Cross-correlating real datasets is technically challenging: the “footprints” of different surveys must overlap in both angular and redshift space. In 21-cm interferometry, foregrounds combined with the instrument response contaminates a “wedge” region in Fourier space (e.g. Liu and Tegmark 2011; Vedantham et al. 2012; Morales et al. 2012). The remaining so-called "EoR window" spans large transverse scales combined with small line of sight scales (i.e. low $k_{\perp}$ + high $k_{||}$). Hence, ideal cross-correlation partners are large-volume surveys with accurate redshift localization. Possible candidates for cross-correlations include:

1. *Cosmic backgrounds* — Integrated backgrounds such as the CMB, NIR, and X-ray backgrounds include emission from $z > 5.5$ and should correlate with the EoR/CD 21-cm signal (e.g. Ma et al. 2018a; Zhou et al. 2025). However, their broad redshift integration limits overlap with 21-cm modes lost to foreground removal.

2. *Resolved galaxies* — Galaxy maps are natural 21-cm counterparts, but surveys at $z > 5.5$ must balance wide fields, accurate redshifts, and sufficient source densities. Narrow-band

dropout techniques, grism surveys, and slit spectroscopic follow-ups are the most promising approaches (e.g. Vrbanec et al. 2020; Heneka and Mesinger 2020; Hutter et al. 2023a).

3. *Line Intensity Mapping (LIM)* — Mapping of lines such as [C II], [O III], CO, and Ly$\alpha$ can trace the combined emission from unresolved galaxies. LIM offers large volumes and good redshift precision, making it an ideal complement to 21-cm tomography (e.g. Kovetz et al. 2017). However, LIM observations at high redshift remain untested, and expected line luminosities are faint (e.g. Yue et al. 2015)

4. Quasar spectra — The Lyman-$\alpha$ forest in quasar spectra can be cross-correlated with the 21-cm forest, providing complementary UV and radio absorption probes of the same IGM regions (Bhagwat et al., 2022). This requires radio-loud quasars at high redshift and a sufficiently cold IGM for 21-cm absorption.

In this chapter we review the current state of synergies, highlighting how they are shaping our knowledge of EoR galaxies and the IGM. We also discuss future potentials for cross-correlation with the cosmic 21-cm signal. We end with a summary of early science targets that could be used to make and verify the first 21-cm detection of the EoR with SKA.

## 2 Informing our understanding

In this section we discuss how multi-wavelength studies of the EoR are shaping our understanding of the dominant physical processes.

### 2.1 The nature of sources

The sources of reionization remain a key outstanding issue in the field (see reviews in, e.g., Mesinger 2016; Dayal and Ferrara 2018). This is because the relative contributions of sources (including low versus high-mass star-forming galaxies and black holes) depend on a number of poorly understood parameters including *(i)*: the halo-mass dependence of star formation and black hole accretion; *(ii)*: intrinsic stellar populations (star formation history, initial mass function, metallicity) that determine the output of ionizing photons; *(iii)*: the line-of-sight and galaxy property dependent escape fraction of Lyman continuum photons into the IGM ($f_{\rm esc}$); and *(iv)*: the clustering of sources that determines both the reionization morphology and its feedback on the baryonic contents of low-mass halos.

The James Webb Space Telescope (JWST) has been transformational in extending constraints on the star-forming galaxy population well within the first billion years between $z \sim 10-15$ (Adams et al., 2024; Harikane et al., 2024; Donnan et al., 2024) with even some preliminary estimates of the ultra-violet luminosity function out to $z \sim 15-20$ (Kokorev et al., 2025; Whitler et al., 2025; Castellano et al., 2025), going down to systems with absolute UV magnitudes as faint as $M_{\rm UV} \sim$ -15 to -17 i.e. $0.005L_*$ (Atek et al., 2024). We also have tentative hints on the stellar mass functions (Weibel et al., 2024; Harvey et al., 2025), mass-metallicity relations (Curti et al., 2024; Chemerynska et al., 2024) and UV spectral slopes (Austin et al., 2024; Rinaldi et al., 2024). Together, these build a picture of robustly star-forming, low-metallicity, young systems within the

first billion years. Crucially, JWST observations have also yielded hints on the ionizing photon production efficiency ($\xi_{\rm ion}$ in units of Hz s$^{-1}$) which is the production rate of ionizing photons per unit UV luminosity: while theoretical estimates suggested $\log \xi_{\rm ion} \sim 25.2$, observations imply $\log \xi_{\rm ion} \sim 25.8$ (Simmonds et al., 2024; Begley et al., 2024; Atek et al., 2024). Observational works also imply the $\log \xi_{\rm ion}$ scales inversely with the galaxy luminosity, decreasing from 25.6 to 25 as $M_{\rm UV}$ decreases from $\sim -18$ to $\sim -22$ at $z \sim 5$ (Llerena et al., 2024). Furthermore, the dependence of $f_{\rm esc}$ on galaxy properties (and hence redshift) is one of the most crucial parameters for reionization (e.g. Maity and Choudhury 2022a; Qin et al. 2025). Together, these properties determine not just the EoR morphology but also the distribution of galaxies visible as Lyman Alpha Emitters (e.g. Sobacchi and Mesinger 2015; Hutter et al. 2023b; c.f. Fig. 1). Matching JWST UV luminosity functions at $z \geq 10$, along with data related to reionization history, might point to enhanced star-formation efficiency and halo-mass–dependent escape fractions (e.g. Qin et al. 2025). Depending on the galaxy model, these trends might be in tension with observed galaxy clustering (Chakraborty and Choudhury, 2024, 2025).

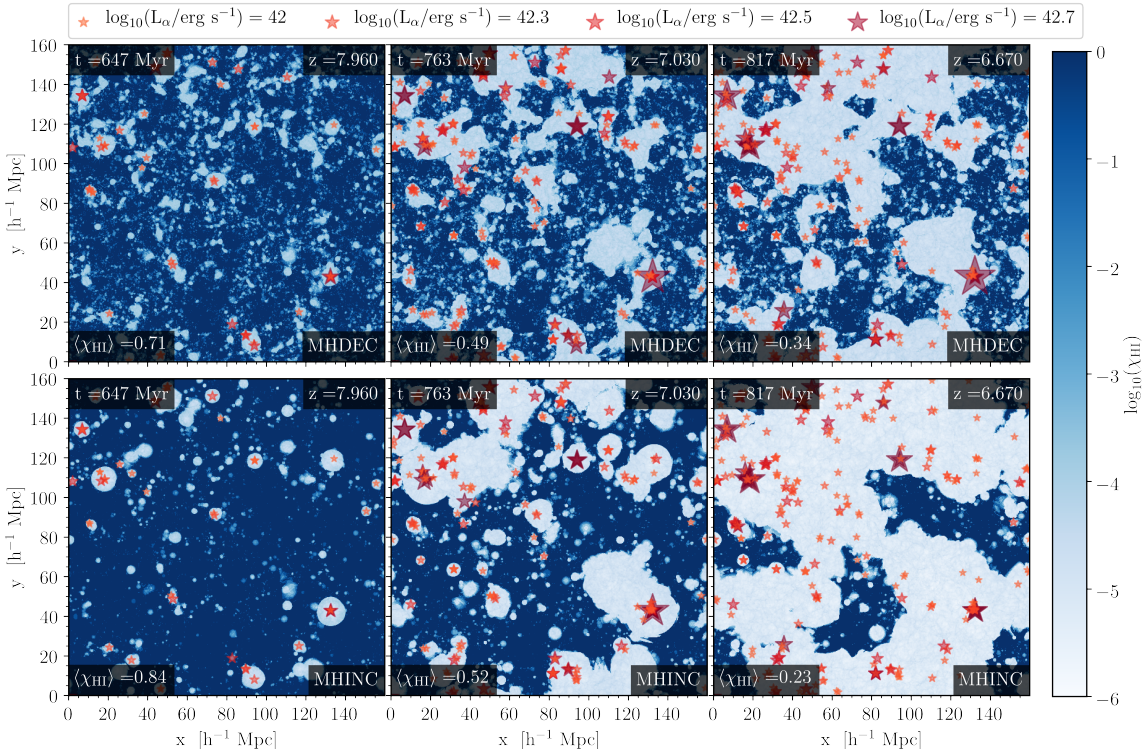


**Figure 1:** The progress of reionization and the associated evolution of Lyman Alpha Emitter (LAE) visibility between $z \sim 8$ and $z \sim 6.6$, from left to right, as marked (Hutter et al., 2023b). The upper and lower rows show results for scenarios in which $f_{\rm esc}$ decreases (MHDEC) and increases (MHINC) with an increase in halo mass, respectively. EoR morphology is much richer in small-scale structures when low-mass sources dominate the process (MHDEC) as opposed to being much more biased when rarer higher-mass sources drive the process (MHINC) (e.g. McQuinn et al. 2007).

JWST observations have also revealed a large population of AGN in the early universe (z>4) which, although fainter, are much more abundant than luminous quasars found by pre-JWST surveys (Maiolino et al., 2024; Taylor et al., 2024). Surprisingly, the luminosity function of

AGN spectroscopically identified by JWST is about one or two orders of magnitude higher the extrapolation of the luminosity function of pre-JWST discovered quasars at $z \sim 5-7$. AGN are estimated to make up a few percent of the galaxy population at the bright end (Greene et al., 2024; Kokorev et al., 2024; Akins et al., 2024; Matthee et al., 2024), contributing up to $18-30\%$ of the UV luminosity function (Scholtz et al., 2025). Such high AGN number densities have prompted a reevaluation of their role in reionization. Models that have AGN dominating the EoR must however make extreme assumptions such as high escape fractions, high occupancy, soft (stellar like) spectra and Compton thick disks (e.g. Madau et al. 2024; Grazian et al. 2024). Most works still credit faint galaxies as dominant sources of the EoR (Robertson et al., 2015; Madau, 2017; Qin et al., 2017; Atek et al., 2024; Dayal et al., 2025; Qin et al., 2025).

Finally, we expect that the heating of the IGM to temperatures exceeding the CMB likely preceded the bulk of the EoR. This was expected given the observed scaling relations between X-ray luminosities and star formation rates in local galaxies (e.g. Fragos et al. 2013; Kaur et al. 2022), and has recently been confirmed observationally using 21-cm upper limits (e.g. HERA Collaboration et al. 2023). This heating is most likely driven by X-rays emitted by metal-poor X-ray binary stars in the first galaxies (Kaur et al., 2022; Sartorio et al., 2023). However, more exotic sources of heating could be provided by accreting primordial black holes (e.g. Dayal 2024; Zhang et al. 2025), decaying dark matter (e.g. Liu and Slatyer 2018; Facchinetti et al. 2024), annihilating dark matter (e.g. Evoli et al. 2014; Lopez-Honorez et al. 2016), or cosmic rays (Sazonov and Sunyaev, 2015; Leite et al., 2017; Jana and Nath, 2018; Gessey-Jones et al., 2023).

### 2.2 The state of the IGM

Prior to direct measurements of the EoR using the 21-cm line, we must rely on alternative probes provided by the damping wing absorption in galaxy and quasar spectra, the Lyman alpha forest, and the CMB. In Fig. 2, we show the latest constraints on the ionization history derived from several different types of measurements. These constraints are roughly consistent with each other, implying an early start to the EoR (e.g. Curtis-Lake et al. 2023; Tang et al. 2024) and a late end extending below $z \sim 6$ (e.g., Kulkarni et al., 2019; Bosman et al., 2022). The maximum-a-posteriori (MAP) model from Qin et al. (2025), inferred from the Lyman alpha forest, combined with UV LFs and the CMB optical depth, is also shown in the figure. While these constraints remain broad, they provide valuable guidance for model development. The figure shows several reionization models developed using different frameworks, including hydrodynamical simulations—`CoDa III` (Lewis et al., 2022) and `Thesan-1` (Garaldi et al., 2022)—and post-processing of dark matter N-body simulations—`pyC`$^2$`2Ray` (Source1_SinkA; Giri et al., 2024), `Meraxes` (L210_AUG; Balu et al., 2023), and `Astraeus` (Evolving IMF; Hutter et al., 2025). However, most simulations must tune their ionizing escape fraction in order to get reasonable EoR histories, limiting their predictive powers.

The thermal history of the IGM has been extensively studied at $z \lesssim 6$ using the Lyman-$\alpha$ forest (Schaye et al., 2000; Theuns et al., 2002; Bolton et al., 2010, 2012; Boera et al., 2019; Walther et al., 2019; Gaikwad et al., 2020; Maity and Choudhury, 2022a,b). Complementary limits on the thermal state of the neutral IGM at $z > 10$ have been derived from 21-cm observations HERA Collaboration et al. (2023), implying an additional source of heating beyond the well-known processes of adiabatic

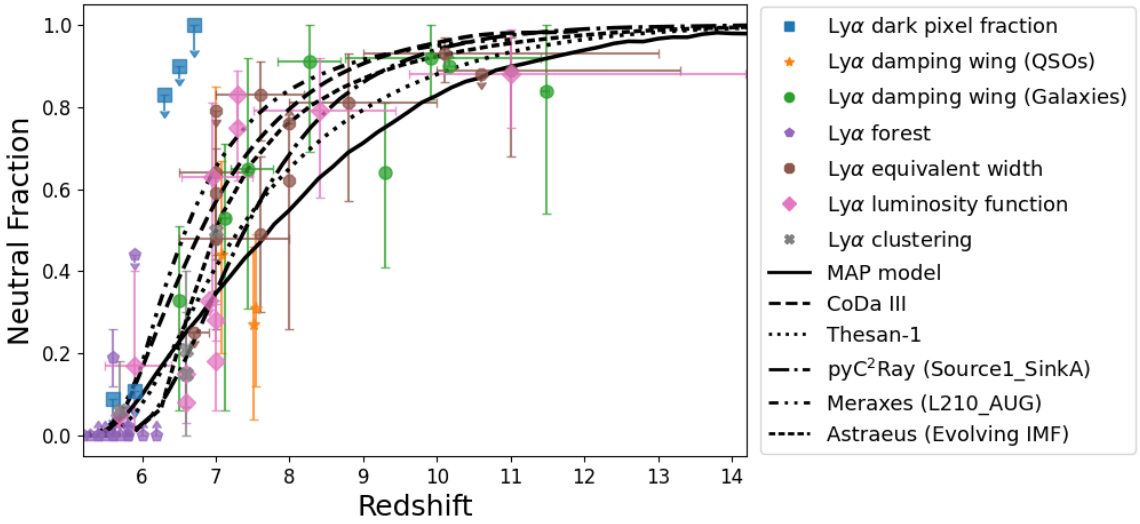


**Figure 2:** Constraints on the reionization history of the intergalactic medium from multiple observational probes. Different Lyman-$\alpha$ observations constrain the ionization fraction as a function of redshift, including: the dark pixel fraction in quasar spectra (McGreer et al., 2015; Jin et al., 2023), Lyman-$\alpha$ damping wing profiles (Greig et al., 2022; Curtis-Lake et al., 2023; Hsiao et al., 2024; Umeda et al., 2024; Mason et al., 2025), the transmitted flux in the Lyman-$\alpha$ forest (Yang et al., 2020; Bosman et al., 2022; Spina et al., 2024; Zhu et al., 2024), Lyman-$\alpha$ equivalent widths (Mason et al., 2018, 2019; Jung et al., 2020; Bolan et al., 2022; Bruton et al., 2023; Nakane et al., 2024; Tang et al., 2024; Jones et al., 2025), the luminosity function evolution of Lyman-$\alpha$ emitters (Inoue et al., 2018; Morales et al., 2021; Wold et al., 2022; Umeda et al., 2025; Kageura et al., 2025), and their spatial clustering properties (Sobacchi and Mesinger, 2015; Ouchi et al., 2018; Umeda et al., 2025). We show the maximum-a-posteriori (MAP) model from Qin et al. (2025) that was inferred from Lyman alpha forest data, together with UV LFs and the CMB optical depth. State-of-the-art numerical simulations, including `CoDa III` (Lewis et al., 2022), `Thesan-1` (Garaldi et al., 2022), `pyC`$^2$`Ray` (Source1_SinkA; Giri et al., 2024), `Meraxes` (L210_AUG; Balu et al., 2023), `Astraeus` (Evolving IMF; Hutter et al., 2025), are consistent with these observational constraints.

and Compton cooling/heating.

### 2.3 Inference using complementary data

Complementary datasets are essential for constraining the state of the IGM during the EoR. They help in breaking degeneracies among key astrophysical parameters and provide independent insights into different phases and components of the reionization process. In recent years, there has been a surge in EoR-relevant observations across a wide range of probes (see some examples in Fig. 2), including:

1. primary and secondary anisotropies of the cosmic microwave background (CMB; Planck Collaboration et al. 2016; Reichardt et al. 2021)
2. the large-scale fluctuations in Lyman-alpha forest trasmission (Fan et al. 2006; Bosman et al. 2022) and its associated dark gaps (Mesinger, 2010; Zhu et al., 2021);
3. the damping-wing absorption in high-redshift quasar (Greig et al., 2017; Bañados et al., 2018; Davies et al., 2018) and galaxy spectra (Curtis-Lake et al., 2023; Umeda et al., 2024);

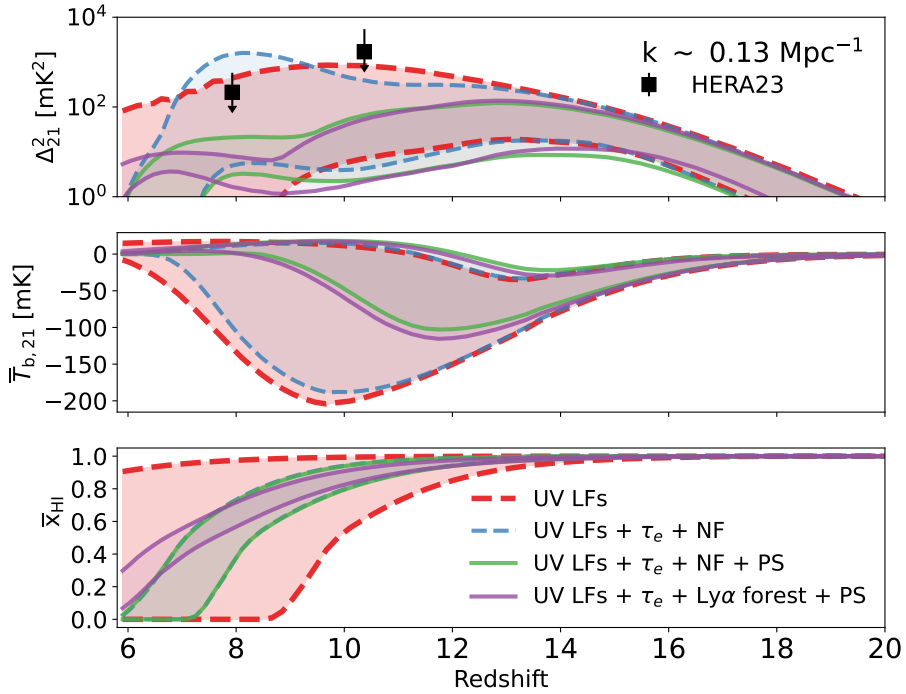


**Figure 3:** Constraints on the redshift evolution of the 21-cm power spectrum at $k = 0.13$ cMpc$^{-1}$, the 21-cm global signal and mean neutral fraction, top to bottom. The shaded regions and areas enclosed between paired curves indicate 95% confidence intervals inferred from different combinations of observational probes, including the high-redshift galaxy UV luminosity functions (UF LFs), CMB optical depth ($\tau_e$), neutral/dark fraction (NF) or Lyman-$\alpha$ (Ly$\alpha$) forest statistics from high-redshift quasar spectra, and the latest 21-cm power spectrum upper limits from HERA Collaboration et al. (2023, PS). This figure is obtained using the `21cmFAST` simulation code (Mesinger et al., 2011; Murray et al., 2020), and adapted from Breitman et al. (2024).

4. the luminosity functions of broad band dropouts (Inoue et al., 2018; Morales et al., 2021), and Lyman-alpha emitters (Sobacchi and Mesinger, 2015; Ouchi et al., 2018);

5. upper limits on the 21-cm power spectrum from radio interferometers (Trott et al., 2020; HERA Collaboration et al., 2023; Mertens et al., 2025; Nunhokee et al., 2025).

Theoretical frameworks have advanced in parallel, with different approaches ranging from analytic to semi-numerical to full radiative transfer simulations (see a couple of examples in Fig. 2). These frameworks aim to capture inhomogeneous reionization driven by physically motivated galaxy formation models, and are increasingly capable of integrating multiple complementary probes in their inference pipelines.

What do these datasets imply for the evolution of the IGM and the corresponding 21cm signal? In Figure 3 we show four inference results, varying which datasets are included in the likelihood: (i) UV luminosity functions (UV LFs) of galaxies alone (Bouwens et al., 2015, 2016; Oesch et al., 2018); (ii) CMB optical depth (Planck Collaboration et al., 2016; Qin et al., 2020) and Dark Fraction upper limits on the neutral hydrogen fraction (McGreer et al., 2015), in addition to the UV LFs;

(iii) 21-cm power spectrum upper limits from HERA (HERA Collaboration et al., 2023), included in addition to the above; (iv) substituting the Dark Fraction with the latest measurements of the Lyman alpha effective optical depth (Bosman et al., 2022; Qin et al., 2025).

The UV LFs alone rule out extreme scenarios in which the IGM is heated or ionized either too early or not at all. Adding the CMB optical depth and Dark Fraction constrains the neutral fraction evolution, restricting the reionization mid-point to a narrower window of $7 < z < 8$. While this combination impacts the positive envelope of the mean 21cm signal (when it is in emission), and so is difficult to see in the figure in which the dynamic range of the mean signal is dominated by the absorption trough, we do see a large impact on the 21cm power spectrum. This is especially notable at $z < 7$, by excluding models that reionize too early or too late.

In contrast, the inclusion of current 21-cm PS upper limits from HERA does not significantly alter the inferred ionization history, but substantially tightens the posterior on the 21cm brightness temperature. These limits effectively rule out "cold reionization" models (Mesinger et al., 2014) in which the neutral IGM patches are significantly colder than the CMB (or other) radio background, and thus provide a strong brightness temperature contrast with the ionized IGM patches during the EoR, resulting in a high amplitude power spectrum. Finally, replacing the Dark Fraction with the most recent Lyman alpha effective optical depth measurements not only shifts the posterior distribution of the neutral fraction but also leads to noticeable changes in the resulting 21-cm PS, reflecting the updated understanding of the timing of reionization. With a peak in the 21cm power spectrum at later times, where instrumental noise is lower, there appears to be a growing opportunity to detect the 21-cm power spectrum in the near future.

Observations of present-day radiation backgrounds, including the X-ray background observed by Chandra and the radio background observed by ARCADE, can provide additional constraints on the galaxy population during the EoR and CD. These are broadly consistent with the constraints above, but can additionally disfavor very early heating and strong radio excess (e.g. Dhandha et al. 2025b,a), with the caveat that connecting the high-$z$ population to the $z = 0$ background is sensitive to the assumed X-ray and radio spectral energy distributions (e.g. Mirocha et al. 2025; Katz et al. 2025).

## 3 Statistical cross-correlation

As mentioned in the introduction, cross-correlating early SKA data with other observations will be important as a sanity check for first claims of a detection as well as helping mitigate unknown systematics. Here we discuss possible targets for such cross-correlation studies, commenting on their detectability.

### 3.1 Cosmic Background Radiation

#### *3.1.1 CMB*

We have seen in Sec. 2.3 that measurements of the large-scale CMB polarisation and temperature power spectra can be combined with astrophysical and 21 cm measurements to sharpen our picture of the reionisation history (Qin et al., 2020). Indeed, fluctuations in the electron density during

reionization lead to distinct scaling relations in both the patchy–kSZ and B-mode signals – relations that, when combined with 21 cm observations, can robustly break degeneracies between optical depth, reionization duration, and bubble morphology (Paul et al., 2021).

**Thomson scattering.** Thomson scattering of CMB photons off electrons produced by reionisation dampen CMB temperature anisotropies and enhance its polarisation anisotropies. Through this effect, many CMB observables can be cross-correlated with 21 cm observations to isolate the reionisation contribution in both signals. Tashiro et al. (2008) have shown that the cross-correlation of CMB $E$-mode polarisation anisotropies with 21 cm brightness fluctuations, on large scales, can accurately constrain the reionisation history: the peak of the cross-correlation spectrum is maximum when about half of the IGM is ionised, and there is a damping in the spectrum that depends on the duration of reionisation. However, the faintness of the signal makes it difficult to observe with experiments such as LOFAR and Planck (Tashiro et al., 2010). Only an ambitious survey carried out with the SKA-*Low*, where several fields are observed for 1000 hours to cover 2% of the sky could lead to a signal-to-noise ratio of one – and this is ignoring residual foregrounds and systematics polluting the cross-signal.

The patchiness of the reionisation process leads to spatial fluctuations in this optical depth which can be leveraged to constrain reionisation morphology. We expect a lot of information about reionisation to be enclosed in the spatial fluctuations of $\tau$ (Dvorkin and Smith, 2009; Gluscevic et al., 2013; Meerburg et al., 2017). Their study has been gaining momentum in the past few years, namely as a tracer of post-reionisation large-scale structures (Schutt et al., 2024). The detectability of these fluctuations has been established in the literature, either alone, with telescopes such as the now canceled CMB-Stage 4, or of even better sensitivity, such as CMB-HD (Roy et al., 2018, 2021); or sooner in cross-correlation with, e.g., gravitational lensing with SPT-3G (Bianchini and Millea, 2023). During reionisation, spatial fluctuations in $\tau$ and in the 21 cm signal are expected to be anti-correlated, as scattering comes from ionised regions whilst 21 cm brightness stems from neutral Hydrogen (Holder et al., 2007). Some works in the literature have shown the anti-correlation shape and amplitude to depend not only on the reionisation history, but also on the details of the physics of reionisation, such as ionised bubble sizes (Meerburg et al., 2013; Roy et al., 2020). Assuming that the measurement is limited by instrumental noise and cosmic variance rather than foregrounds and systematics, Roy et al. (2020) find a cumulative SNR of 11.5 when cross-correlating observations from the SKA and the Simons Observatory, already online, provided observations cover at least 10% of the sky. Additionally, the reionisation patchiness leads to the production of faint $B$-modes, which are directly related to $C_\ell^{\tau\tau}$, and, thus, trace reionisation history and morphology (Mukherjee et al., 2019; Choudhury et al., 2021; Roy et al., 2021; Jain et al., 2023, 2024). Despite similar arguments as $\tau \times 21$ cm correlations, so far, no forecast for the measurements of 21 cm $\times$ EoR-induced $B$-modes angular cross-spectra has been performed.

**The kinetic Sunyaev-Zel'dovich effect.** CMB photons can interact with electrons from reionisation that have a bulk velocity with respect to the CMB rest-frame through a Doppler shift process known as the kinetic Sunyaev-Zel'dovich (kSZ) effect. Additional temperature anisotropies are produced by this interaction, both on large scales (Alvarez et al., 2006; Adshead and Furlanetto, 2008) and at scales corresponding to the typical size of ionised bubbles during reionisation (multipoles

$\ell \sim 3000$). Extensive work has been performed to forecast the potential of cross-correlating this signal with 21 cm brightness temperature, both with numerical simulations (Salvaterra et al., 2005; Jelić et al., 2010; Mesinger et al., 2012; La Plante et al., 2020) or analytical models (Cooray, 2004; McQuinn et al., 2005; Tashiro et al., 2011). In every configuration, the cross-signal is found to be a good tracer of reionisation history and morphology, mainly through its shape and sign flips, as well as potentially of cosmic magnetism (Kunze, 2023). On large scales, although Tashiro et al. (2010) have found the signal to be detectable with a cumulative SNR of about 10 (2) for a combination of Planck and SKA (LOFAR) data, a detection has not yet been achieved, namely because of strong foreground pollution in the 21 cm data, as demonstrated for MWA observations in Yoshiura et al. (2019). Such observations on very large scales (several degrees) would be limited by the smaller field-of-view of the SKA. On smaller scales, the anti-correlation traces the size of ionised bubbles as it is stronger for larger bubbles, and peaks at a multipole one can relate to the typical bubble size (Salvaterra et al., 2005; Jelić et al., 2010; Tashiro et al., 2011). However, the signal is overall faint as ionised regions are equally likely to be moving towards or away from the observer[1] (Alvarez et al., 2006). Different options have been discussed in the literature to limit this effect:

- Cross-correlating kSZ and 21 cm maps that have been integrated over the line of sight. However, since the homogeneous (patchy) kSZ anisotropies (anti-)correlate with the 21 cm signal, the two contributions tend to cancel each other (Jelić et al., 2010).

- Two-point correlations after squaring the kSZ signal – making sure the primary CMB component and other sources of unwanted noise are filtered out before performing the squaring. In the absence of 21 cm foregrounds, this signal is detectable at the $\gtrsim 35\sigma$ level for 10 hours of integration time with the SKA (Ma et al., 2018b). Zhou et al. (2025) have more recently proposed to also square the 21 cm signal to compensate for a filter applied to remove the brightest foregrounds contributions whilst retaining cosmological information. Such a signal will also be detectable with a combination of SKA and Stage 3 CMB experiments, such as SO or SPT-3G.

- Three-point correlations, two points being taken in the kSZ field[2] (Cooray, 2004), whose intensity is related to the reionisation history. In the absence of foreground contamination, this signal is detectable with SKA and SO – at more than $20\sigma$ for the cumulative signal (La Plante et al., 2020). However, the kSZ signal is sensitive only to Fourier modes with long-wavelength line-of-sight components, which are most strongly polluted by foregrounds in 21 cm data sets.

Overall, a wealth of information is enclosed in the kSZ×21 cm signal, which is highly detectable by the SKA in combination with both current and future CMB experiments, in a framework where uncertainties are dominated by noise. Further work must be carried out to assess the true detectability of the signal – and reach detection, e.g., taking into account detailed foreground mitigation techniques, both in CMB and in 21 cm data analysis.

[1] This cancellation is partially avoided on large scales, where the signal is, however, fainter (Adshead and Furlanetto, 2008; Ma et al., 2018b).

[2] Note that this statistic is related to the previous one by a simple integral.

### *3.1.2 The near infrared background*

The cumulative ionising (UV) light of faint galaxies at $z \sim 10-20$ could form background radiation, redshifted to infrared frequencies. Sun et al. (2021b) have shown that Pop III stars can leave characteristic spectral signatures on this near infrared background (NIRB) spectrum, depending on the conditions of their formation. Observed by SPHEREx, such features could provide constraints on the abundance and formation history of Pop III stars at high redshifts.

The NIRB and the 21cm signal trace opposite phases of the IGM on large scales during reionisation (we expect them to be to be anti-correlated) and can be combined to provide powerful constraints on the reionisation history, as the NIRB alone cannot provide redshift information (Shan and Qin, 2009; Mao, 2014; Fernandez et al., 2014). However, the cross-signal is difficult to access in observations as NIRB fluctuations probe large-scale modes which are dominated by foregrounds in 21 cm data. Similarly to what has been proposed for CMB cross-correlations, the 21 cm signal can be squared after filtering out foreground-dominated modes and before cross-correlating it to the NIRB. The resulting signal, related to the 21-21-NIRB bispectrum, traces the reionisation history and can be detected at high significance by the SKA and SPHEREx (SNR= 6.8 at $z = 9$ when observing for 1000 hrs with SKA-*Low*, see Sun et al., 2025).

### *3.1.3 The X-ray background*

As discussed above, we expect the IGM to be heated to temperatures above the CMB, driving the signal from absorption to emission, before the bulk of the EoR. The sources responsible could include X-ray emission from X-ray binaries, AGNs, and shock heated interstellar medium. However, these sources are hardly detectable in the cosmic X-ray background (CXB) radiation permeating our Universe, as they represent less than a few percents of its mean intensity and spatial fluctuations (Ma et al., 2018a). The cross-correlation of the CXB with the 21 cm signal helps in isolating the EoR/CD contribution to the CXB and contains information on the properties of the X-ray sources and the timing of these epochs (Shan and Qin, 2009; Liang et al., 2016). This cross signal could be detectable if the X-ray survey is deep enough to remove bright sources with an observed flux $\geq 10^{-17}$ erg/cm$^2$/s, whilst covering a wide field of view (Ma et al., 2018a). In this respect, we expect a cumulative SNR $\gtrsim 1$ when cross-correlating SKA data with observations carried out with the Wide Field Imager (WFI) of the upcoming space telescope *New*Athena (Cruise et al., 2025).

## 3.2 Resolved Galaxies

This section highlights the prospects for statistical cross-correlation of the 21cm signal and galaxy maps. Galaxy surveys are ideal candidates for cross-correlation with the large-scale 21cm signal due to the potentially wide fields they probe. The range of galaxy survey experiments most promising for detection includes narrow-band dropout, slitless spectroscopy and slit spectroscopic followup. The 21cm-galaxy cross-correlation signal is sensitive to the progress of reionization, its topology, and the heating state of the IGM – while also encoding ensemble properties of galaxy populations and their environments. Studies have focused on 1) the detectability of the signal depending on survey characteristics and 2) the signal sensitivity to and dependence on reionization parameters and source properties.

### *3.2.1 Survey characteristics and detectability of the 21cm-galaxy cross-correlation*

Emission lines are needed for redshift localization of galaxies as well as to efficiently detect them without expensive spectroscopic campaigns. Galaxies with strong emission lines are most the most promising candidates, such as Lyman-alpha emitters (LAE), as well as H-alpha and [OIII] emitters. For cross-correlation with the SKA, several studies have focused on signal shape and detectability of the 21cm-LAE cross-correlation, particularly for LAEs detected via narrow-band dropout with Subaru Hyper-Suprime Cam (HSC; Sobacchi et al., 2016; Hutter et al., 2017; Kubota et al., 2018, 2020; Heneka and Mesinger, 2020; Gagnon-Hartman et al., 2025), driven by ongoing measurements of comparably wide fields at redshifts $z \sim 5.7, 6.6, 7.3$. Fig. 4 (left panel) shows a sketch of the dependency of the signal overlap region for the 21cm-galaxy cross-correlation on the galaxy survey redshift uncertainty, $\sigma_z$, its field-of-view (FoV), and the 21cm foreground contamination. The smaller the $\sigma_z$, the larger the FoV, and the less extended the foreground wedge, the larger the signal overlap in cross-correlation. These studies consistently report that during the EoR, the amplitude of the cross-correlation function, or coefficient, generally decreases (increases) with the ionized (neutral) fraction of the IGM $x_{\rm HII}$ ($x_{\rm HI}$) and is negatively correlated in the post-heating regime, when the IGM is, on average, hotter than the CMB and spin temperature fluctuations saturate. The strongest (anti-)correlation signal occurs at small scales (< few cMpc) as ionized regions around LAEs appear as cold spots. At large scales the cross-correlation coefficient becomes approximately zero, see Fig. 6 (right panel). For fiducial SKA1-Low 1000h observations, both for AA* and AA4 antenna configurations, the anti-correlation at small to intermediate (few tens of cMpc) scales has been reported to be detectable, depending on the assumed galaxy survey characteristics. This makes it possible to track the progress of reionization by distinguishing between different average HI fractions of the IGM. We note that the S/N achievable also critically depends on the foreground model adopted for SKA1-Low.

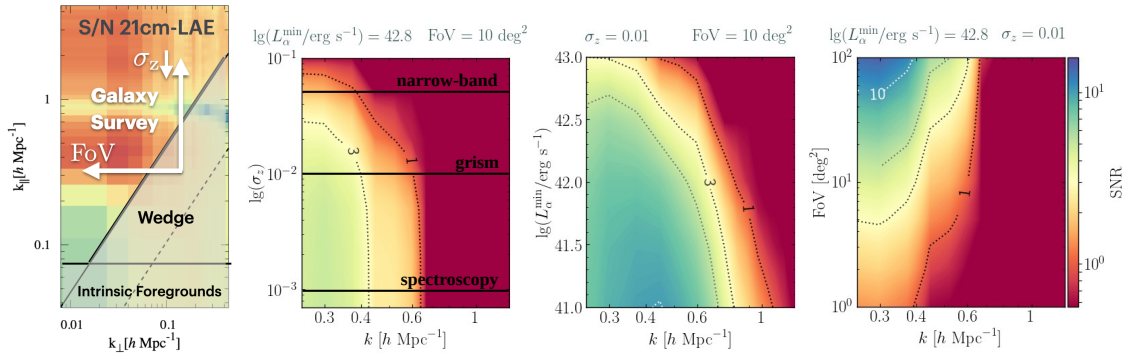


**Figure 4:** Left panel: Example of the 2D 21cm-galaxy cross-correlation S/N. The signal overlap region in k-space depends on galaxy survey redshift uncertainty and survey area, as well as SKA1-Low foreground assumptions (Yoshiura et al., 2018); Right panels: the S/N as a heatmap for the spherical 1D 21cm-galaxy cross-correlation PS for given survey specifications (y-axis) as a function of k (x-axis), assuming 1000 h SKA1-low noise in AA4 configuration (Heneka and Mesinger, 2020; Hutter et al., 2023b) and optimistic foregrounds. Shown are from left to right the impact on the S/N for a) redshift uncertainty, b) luminosity threshold, c) FoV.

In Fig. 4, the three right panels show, from left to right, the S/N dependence as a heatmap for the

spherical 1D 21cm-galaxy cross-correlation PS, for a range of realistic galaxy survey specifications and noise for 1000 h SKA1-low in AA4 configuration. First, we note that across survey characteristics accessible k-modes range from $\sim 0.2$ to $\sim 1\,\mathrm{Mpc}^{-1}$. Regarding the dependence on $\sigma_z$, both slitless (e.g. grism) and slit spectroscopic surveys similarly enable measurements with S/N > 3, and narrow-band surveys reach S/N > 1 across several k-bins for a fiducial $10\,\mathrm{deg}^2$ field, well within reach for for narrow-band and grism observations. As for $\sigma_z$ we note a relatively mild dependence on the range of luminosity thresholds or survey depths (middle), but a stronger dependence on the survey FoV (right). For slitless and slit spectroscopic FoV $\gtrsim$ multiple $100\,\mathrm{arcmin}^2$ to 1 deg are desirable, whereas narrow-band surveys are expected to require FoV > $10\,\mathrm{deg}^2$ for significant detections.

Several studies have extended their analysis to the cross-correlation with the 21cm signal for spectroscopically confirmed LAEs via Subaru Prime Focus Spectrograph (PFS) follow-up, VLT MOONS, and ELT MOSAIC slit spectroscopy, as well as grism observations with the Roman Space Telescope (Hutter et al., 2018; Vrbanec et al., 2020; Gagnon-Hartman et al., 2025). Here, grism and slit spectroscopy can significantly enhance detectability and S/N of the cross-signal due to the reduced redshift uncertainty, even at moderate survey depths and survey areas of a few degrees. Besides LAEs, H-alpha ($z < 7$), [NII] ($z \sim 6$), H-beta and [OIII] ($z > 7$), and [OII] ($z \sim 10$) line-emitting galaxies are also potentially high S/N tracers for the creation of galaxy maps and cross-correlation with the 21cm signal. For example, surveys with JWST NIRCam, using either grism modules or narrow-band filters, are suitable candidates (Moriwaki et al., 2019). We note however, that the S/N of the cross-correlation is sensitive to the assumed 21cm foreground model. In Fig. 5 we show the S/N dependency for specific galaxy surveys (vertical lines) in two foreground wedge scenarios, a) modes below the horizon plus a 0.1 $h\,\mathrm{Mpc}^{-1}$ buffer are excluded (upper panels) b) all modes larger than the beam are recovered (lower panels).

### *3.2.2 The 21cm-galaxy cross-signal as a probe of reionization and source properties*

For the 21cm-galaxy cross-correlation signal during the EoR, studies often rely on either full hydrodynamical and radiative transfer simulations or semi-numerical simulations coupled with (semi-)analytic and radiative transfer recipes to jointly model both the large-scale 21cm signal and line-emitting galaxies.

Across modeling approaches, studies agree that the 21cm-galaxy cross-correlation function is sensitive to HI fraction and distribution in the IGM, with its amplitude generally depending on the progress of reionization and its shape serving as a measure of the reionization morphology (i.e., the size and distribution of ionized regions); examples for modeled LAE and [OIII] emitter x 21cm fields, as well as the signal dependence on the HI fraction are shown in Fig. 6. Additional information is encoded on the reionization morphology; the cross-correlation amplitude at small scales decreases with increasing correlation between the density field and the ionizing emissivity of the galaxy population as traced by ionization. This means that the small-scale amplitude is reduced if lower-mass galaxies drive reionization. The sign and amplitude of the cross-correlation coefficient also depend on the temperature of the neutral IGM (Fig. 5, left panel). Here, an IGM colder than the CMB results in a positive correlation, while in the post-heating regime (saturated spin temperature), the correlation becomes negative, as shown for LAEs in Heneka and Mesinger (2020) and [OIII]

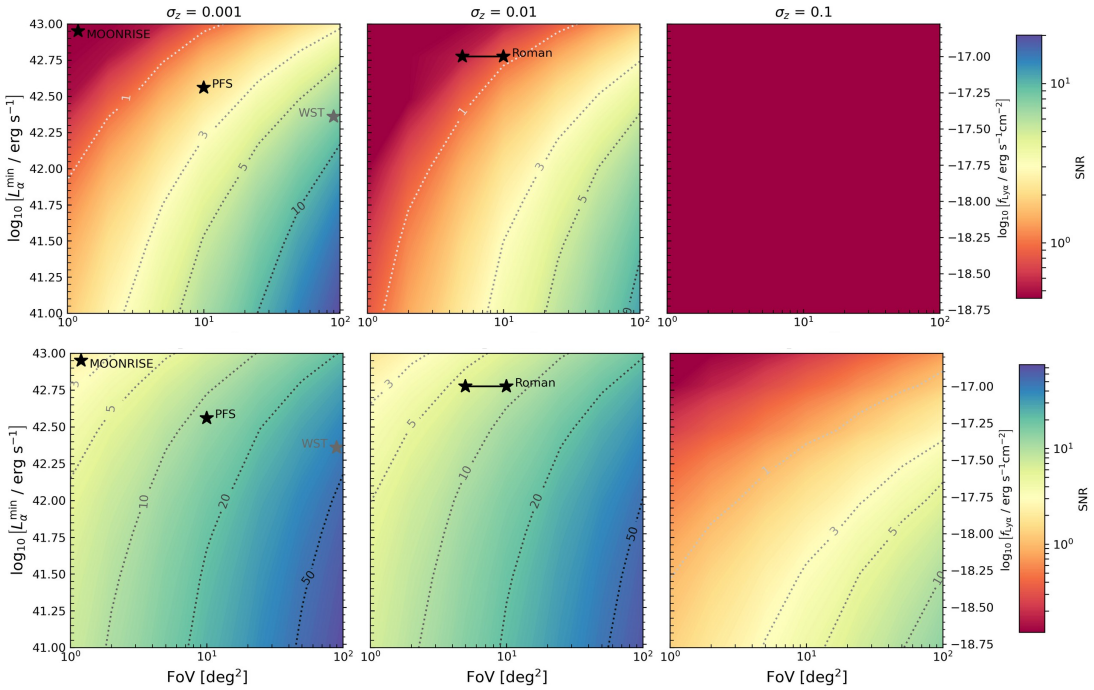


**Figure 5:** Cumulative SNR of $z \simeq 7$ galaxy–21cm cross-power spectrum detection depending on FoV and depth, for slit spectroscopic (left column), grism (middle column), narrow-band (right column) galaxy surveys and two 21cm foreground scenarios, moderate (upper panels) and optimistic (lower panels), see also Gagnon-Hartman et al. (2025).

emitters in Moriwaki et al. (2019). Finally, the cross-correlation, like the galaxy auto-correlation, depends on ensemble properties of galaxies – such as luminosities (where the resulting correlation signal is determined by the luminosity threshold or depth of the survey) and radiative escape through surrounding media, linking intrinsic luminosities associated with star formation rates to observable luminosities.

For LAEs in particular, predictions of the 21cm-LAE cross-correlation from different modeling approaches can be mapped to a common analytical form, exploiting the fact that LAEs are located in sufficiently large ionized regions that allow the Lyman-alpha line to redshift out of resonant absorption. In detail, the small-scale (< few cMpc) cross-correlation amplitude directly scales with both the average HI fraction in the IGM and the spin-temperature-weighted overdensity in neutral regions. While previous studies have also noted that the typical size of ionized regions is related to the inversion point of the cross-correlation function, in Hutter et al. (2023a), the distribution of ionized region sizes and its cumulative distribution function, corresponding to the average profile of the HI fraction around LAEs, was shown to determine the shape and inversion point of the 21cm-LAE cross-correlation.

### 3.3 Multi-wavelength Line Intensity Mapping (LIM)

The bright spectral line emissions from the galaxies, such as [CII] 158$\mu$m (Gong et al., 2012; Silva et al., 2015; Yue et al., 2015; Lagache et al., 2018; Yue and Ferrara, 2019; Sun et al., 2021a;

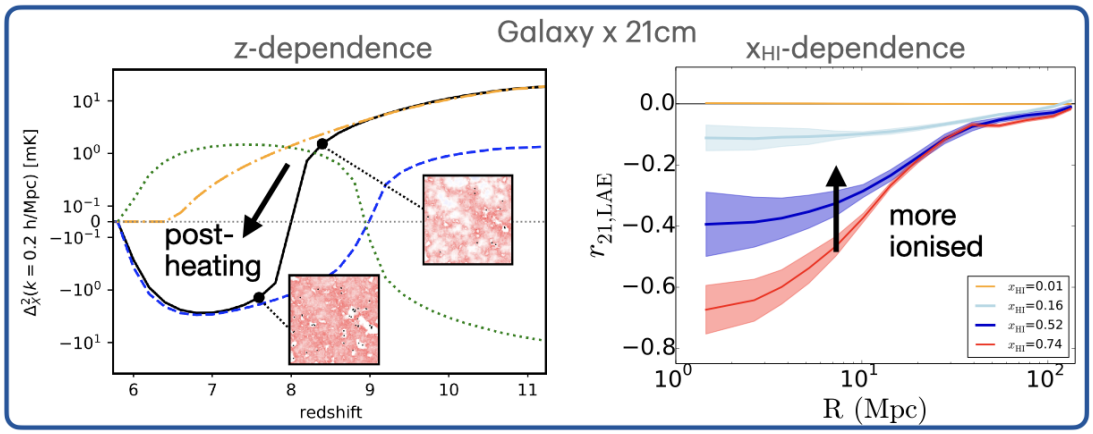


**Figure 6:** Left panel: The redshift evolution of the cross-power spectra between galaxies and fluctuations in the 21cm intensity (black solid), neutral fraction (blue dashed), gas temperature (orange dash-dotted), and matter density (green dotted) (Moriwaki et al., 2024); right panel: cross-correlation coefficient between galaxies and 21cm signal as a function of distance $R$ for different $x_{\mathrm{HI}}$ values (Heneka and Mesinger, 2020).

Béthermin et al., 2022; Moradinezhad Dizgah et al., 2022; Yang et al., 2022; Kannan et al., 2022; Karoumpis et al., 2022; Padmanabhan et al., 2022; Murmu et al., 2021, 2022, 2023; Sun et al., 2023; Van Cuyck et al., 2023; Karoumpis et al., 2024; Liang et al., 2024; Liu et al., 2024; Casavecchia et al., 2025), CO (Carilli, 2011; Lidz et al., 2011; Mashian et al., 2015; Breysse and Rahman, 2017; Breysse et al., 2022; Chung, 2023; Dosibhatla et al., 2025), Ly-$\alpha$ and H-$\alpha$ (Silva et al., 2013; Pullen et al., 2014; Heneka et al., 2017; Silva et al., 2018; Visbal and McQuinn, 2018; Chang et al., 2019; Heneka and Cooray, 2021; Kannan et al., 2022; Mas-Ribas et al., 2023; Sun et al., 2023; Padmanabhan and Loeb, 2024; Lee et al., 2025), [OIII] 88$\mu$m (Padmanabhan et al., 2022), etc., can be good candidates to conduct galaxy LIM, which detects the integrated flux from the numerous unresolved galaxies within voxels. It is therefore similar to the concept of intensity mapping of 21cm emission, originating from the diffuse IGM during the EoR (Furlanetto et al., 2004; Bharadwaj and Ali, 2005), with the difference that the sources of line-emission are discrete in nature (galaxies). LIM has the advantage that it can probe large volumes of the Universe with accurate redshift localization, compared to the traditional galaxy surveys. This implies that galaxy LIM surveys are ideally suited for synergies with large-scale 21cm intensity mapping surveys for which foregrounds contaminate transverse modes making overlapping redshift footprints essential (Lidz et al., 2011; Gong et al., 2012; Heneka et al., 2017; Murmu et al., 2021, 2022, 2023; Kannan et al., 2022; Sun et al., 2021a, 2023; Fronenberg and Liu, 2024).

### *3.3.1 Motivation for multi-tracer LIM*

Intensity mapping of the EoR using the redshifted 21cm signal is essentially a probe of the IGM and its evolution with cosmic time. However, 21cm intensity maps do not provide a direct probe of the sources of reionisation. Thus, a direct probe of the sources of reionisation, the majority of which are expected to be extremely faint galaxies and thus cannot be detected via the usual galaxy surveys, is essential to obtain a complete picture of the EoR. Without a direct probe of the sources of EoR, one will face challenges in constraining the EoR with 21cm maps alone, due to the inherent

degeneracies in reionisation parameters (e.g. Greig and Mesinger 2015; Ghara et al. 2021). Here, LIM of galaxies through their bright spectral lines comes to our rescue as they complement the IGM 21cm maps and thus help in breaking the degeneracies in reionisation model parameters.

Going from smaller to tentatively larger scales probed by multi-wavelength LIM, the H-$\alpha$ line probes the SFR integrated over galactic luminosities of stellar origin, but can be obscured by dust. In optical wavelength, the [OIII] line probes emission from star formation as a tracer of HII regions (Kovetz et al., 2017). The [CII] 158$\mu$m line observed in FIR originates from various phases of the ISM within the galaxies, such as the molecular phase, atomic, and ionised gas (De Looze et al., 2014; Leung et al., 2020). Thus [CII] is also a tracer of the total star formation rate. In the cm/mm to sub-mm regime, the [CO] line emissions arise from the rotational transitions of the CO molecule and they serve as a probe of the molecular gas content in galaxies, which fuels star formation (Carilli and Walter, 2013). Finally, the Ly-$\alpha$ rest-frame UV line potentially probes a multitude of scales; its galactic contribution probes the emission from star formation, and it extends into the CGM through scattering and recombination as a tracer of ionised and partially ionised regions, and even to the IGM – even though at largely decreased intensity – for example due to down-scattering of Ly-n emission. These line emissions, therefore, are probes of different aspects of star-formation, radiative escape, as well as state and properties of gaseous media from the ISM, over CGM, to the IGM, and thus help us shed light on cosmic reionisation. Therefore, multi-wavelength LIM will be essential to probe the EoR.

### *3.3.2 Multi-wavelength LIM experiments*

- **FYST**: The Fred Young Submillimetre Telescope (FYST, CCAT-Prime Collaboration et al., 2023) is well suited to conduct LIM of EoR using the [CII] 158$\mu$m line emission from galaxies. The survey plan suggested by CCAT-Prime Collaboration et al. (2023), relevant for EoR science, can be a survey of two $\sim 4$ deg$^2$ fields, one being the Extended-COSMOS (E-COSMOS, Aihara et al., 2018b) and the other being the Extended Chandra Deep Field South (E-CDFS, Lehmer et al., 2005), including the Hubble Ultra Deep Field (HUDF, Beckwith et al., 2006), with an observation time of $\sim$ 2000 hrs for each field. FYST will have an Epoch of Reionization Spectrometer (EoR-Spec) module, covering frequencies between 210 and 420 GHz and optimized to probe [CII] 158$\mu$m emission over redshifts $3.53 \lesssim z \lesssim 8.05$ (Cothard et al., 2020). Roy et al. (2023) forecasted a cumulative SNR of 4 at $z \sim 7.6$ in their pessimistic scenario for the EoR-Spec of FYST. On the other hand, Clarke et al. (2024) have predicted lower limits on the [CII] 158$\mu$m power spectrum for the EoR-Spec using the COSMOS 2020 galaxy catalogue data (Weaver et al., 2022), which are $\Delta^2(k = 1\,\mathrm{Mpc}^{-1}, 5.34 < z < 6.31) = 9.8 \times 10^5\,(\mathrm{Jy/sr})^2$and $\Delta^2(k = 1\,\mathrm{Mpc}^{-1}, 6.75 < z < 8.27) = 2.77 \times 10^5\,(\mathrm{Jy/sr})^2$. Estimations from works such as Murmu et al. (2021); Karoumpis et al. (2022); Roy et al. (2025) are consistent with the $\Delta^2_{\mathrm{CII}}(k)$ lower limit, placed at $6.75 < z < 8.27$ and $k = 1$ Mpc$^{-1}$. However, models from Kannan et al. (2022) and Sun et al. (2023) are not consistent with these lower limits, where these models predict a lower value of $\Delta^2_{\mathrm{CII}}(k)$, falling in the redshift interval of $5.34 < z < 6.31$ and $6.75 < z < 8.27$, at $k = 1$ Mpc$^{-1}$. To be more precise, Kannan et al. (2022) admits that due to the lack of adequate modelling of [CII] 158$\mu$m emission, their predictions of the line luminosity fall

below those from works such as Lagache et al. (2018) and Leung et al. (2020).

- **TIME**: The Tomographic Intensity Mapping Experiment (TIME) is an imaging spectrometer array that has a wide bandwidth, allowing it to map [CII] 158$\mu$m line emission between redshifts of $6 < z < 9$ (Hunacek et al., 2018; Cheng et al., 2020). With an initial planned observation time of 1000 hrs, it started operation in 2021. Sun et al. (2021a) has forecasted that detection of the [CII] 158$\mu$m power spectrum is possible with SNR $> 5$.

- **COMAP**: The CO Mapping Array Project (COMAP) is designed to detect the CO line emissions from the early Universe (Cleary et al., 2022). It is comprised of a pathfinder instrument having a spectrometer receiver with 19 feeds installed on a 10.4 m diameter dish. The pathfinder instrument can operate between $26-34$ GHz band, thereby targeting the CO(1-0) line from redshifts of $2.4 \lesssim z \lesssim 3.4$ as well as being able to probe the EoR redshifts within a redshift range of $5.8 \lesssim z \lesssim 7.8$ via the CO(2-1) line emission. Therefore, naturally, the CO(1-0) line acts as an interloper for the CO(2-1) line emission from the EoR. Apart from this, the COMAP-EoR instrument, planned to operate in the $12-20$ GHz band, will be sensitive to the CO(1-0) emission out to the EoR. The observation is planned based on three $\sim 4$ deg$^2$ fields having overlap with HETDEX fall and spring fields (Gebhardt et al., 2021). Currently, most of the analysis is focused on extracting the CO(1-0) signal from the post-EoR regime, with the latest work constraining the CO(1-0) power spectrum to $kP_{\rm CO}(k) < 2400 - 4900\,\mu{\rm K}^2\,{\rm Mpc}^2$ in the $k$ range of $0.09 < k < 0.73\,{\rm Mpc}^{-1}$, and in the redshift range of $2.4-3.4$, with 95 percent confidence interval (Stutzer et al., 2024). Although currently, not very many literatures are available showing numerical estimates of the CO(1-0) power spectrum at $2.4 \lesssim z \lesssim 3.4$, the optimistic models from Padmanabhan (2018) suggest that, within their uncertainty range, the maximum predicted $kP_{\rm CO}(k)$ is approximately $\sim 1.6 \times 10^3\ \mu{\rm K}^2\ {\rm Mpc}^2$ at $k \sim 0.7\ {\rm Mpc}^{-1}$, for $z = 3$. On the other hand, Sato-Polito et al. (2023) suggest that their model predicits CO(1-0) power spectrum at $kP_{\rm CO}(k) \sim 360\ \mu{\rm K}^2\ {\rm Mpc}^2$ at $k \sim 0.09\ {\rm Mpc}^{-1}$ and $kP_{\rm CO}(k) \sim 10^3\ \mu{\rm K}^2\ {\rm Mpc}^2$ at $k \sim 0.7\ {\rm Mpc}^{-1}$ for $z = 2.8$. This suggests that the COMAP upper limits at these redshifts are not quite stringent yet. However, both the CO(2-1) and the CO(1-0) signal from the EoR regime still remains to be detected.

- **SPHEREx**: The Spectro-Photometer for the History of the Universe, Epoch of Reionization, and Ices Explorer (SPHEREx, Doré et al., 2014; Crill et al., 2020) is a NASA satellite mission launched in 2025 designed specifically for multi-line intensity mapping to perform an all-sky spectro-photometric survey in the near-infrared. It provides spectroscopic imaging across 0.75 to 5 micron bands in 102 frequency channels at $6.2''$ spatial resolution, enabling detection of key emission lines such as H-$\alpha$, H-$\beta$, [OII], [OIII], and Ly-$\alpha$. Observing these lines across a broad redshift range allows for tracing star formation and galaxy evolution over cosmic time. During the EoR for redshift-overlap and potential cross-correlation with the 21cm background, the mission maps the line intensity of H-$\alpha$, Ly-$\alpha$, and potentially [NII], up to $z \sim 6-8$ depending on the line.

### *3.3.3 Challenges for LIM*

Although the LIM technique can allow for a survey of large cosmological volumes and probe the EoR, it faces certain challenges, one of them being the issue of foreground/interlopers. Given an observation over a certain wavelength range, this band can contain both the signal originating from the target redshift of our interest, and also contaminations from sources at different redshifts. In the case of the 21 cm signal from the EoR, it is known that foregrounds will severely contaminate it (Di Matteo et al., 2002; Santos et al., 2005; Ali et al., 2008), typically by orders of magnitude in terms of signal strength. The sources of foreground in this case could be from galactic synchrotron emission as well as extragalactic radio point sources. On the other hand, for LIM signals like [CII] 158$\mu$m signal originating from the EoR, the CO lines originating from galaxies at much lower redshifts act as interlopers (Gong et al., 2012; Silva et al., 2015).

### *3.3.4 Synergies of 21cm and other multi-wavelength LIMs for probing the EoR*

Cross-correlation of the 21cm observations from IGM with intensity maps of various emission lines from galaxies (originating from the same patch of the sky) e.g. [CO], [CII], [OIII], H-$\alpha$, and Ly-$\alpha$ introduced in Sec. 3.3.1 provides a powerful probe of the reionization process. These cross-correlations are sensitive to the intrinsic properties of the emitters, such as their luminosity-halo mass relation and radiative escape fractions, as well as to CGM/IGM properties. Further, cross-correlation between two independent LIM fields (e.g. 21cm from IGM and [CII] or [CO] from galaxies) observed at different frequencies but originating from the same redshift opens up a unique window to mitigate the effect of foregrounds. The signals from these two LIM fields, originating from the same redshift and from the same piece of sky, are expected to be correlated (positively or negatively, depending on the stage of reionisation and length scale of observation), but their foreground and noise are expected to be uncorrelated and thus will not contribute to the signal cross-power (Lidz et al., 2011; Carilli, 2011). However, foreground removal or avoidance is still necessary, as the residual foregrounds will increase the uncertainty in the estimation of the cross-power (Fronenberg and Liu, 2024).

The cross-power spectrum of [CII]-21cm lines from observations by next-generation experiments e.g. FYST and SKA will be detectable with SNR $\geq$ 10 (Dumitru et al., 2019; Karoumpis et al., 2022, 2024). Such detection, first of all, will act as a confirmatory test for the detection of the cosmic signals from the EoR. Further, the cross-power spectrum will be capable of putting tighter constraints on the minimum halo mass capable of producing Lyman-C photons that can escape galaxies, better than 21cm measurements alone. Additionally, one would be able to constrain the end of reionisation redshift from the sign flip of cross-power at large scales more precisely. However, while inferring the cosmology and astrophysics from the [CII]-21cm cross-power, one should take into account the impact of light-cone effect on this signal statistics, as it can change the cross-power amplitude by $\approx$ 20% or more at large length scales ($k \leq 0.1\,\mathrm{Mpc}^{-1}$) (Murmu et al., 2021). As both of these LIM signals, originating from IGM and galaxies, are inherently non-Gaussian in nature, one can quantify their non-Gaussianity by estimating the cross-bispectrum between them. Beane and Lidz (2018) demonstrated that it would be possible to estimate the redshift evolution of the product of the mean 21cm brightness temperature and 21cm bias using the 21cm-[CII]-[CII] cross-bispectrum. The same can be done with 21cm-Lyman-$\alpha$ cross-bispectrum using the observations

from SPHEREx and HERA, as both have overlapping sky coverage (Doré et al., 2014; Crill et al., 2020; HERA Collaboration et al., 2023; DeBoer et al., 2017). The cross-correlation between the 21cm observation of IGM with the SKA and any other LIM observation from galaxies via FYST, TIME, COMAP and SPHEREx-like instruments has the potential to constrain reionisation history, source models, ionisation morphology and IGM physics in a more robust fashion compared to the auto-correlation of any of these signals alone.

## 4 Image-based synergies

In the previous section we focused on statistical cross-correlations, as will be relevant for initial SKA observations. Eventually with Phase 2, we will be able to study images of individual regions, nailing down the galaxy/AGN – IGM connection. Here we discuss possibilities for such image based synergies.

### 4.1 Galaxies

This subsection describes methods that combine the 21cm signal and galaxy data by directly imaging the 21cm signal around galaxies, including quasars, rather than using cross-correlations. These methods trace quantities similar to those from 21cm-galaxy cross-correlations, such as the sizes of ionised regions and the HI fraction of the IGM, but allow for a more detailed examination of specific environments and galaxy populations. Broadly, they can be divided into two categories: (1) mapping ionised regions around individual galaxies and (2) stacking galaxy-informed 21cm images.

#### *4.1.1 Constraints from mapping ionised regions around galaxies*

The matched filter method, a signal processing technique designed to extract signals from noisy data, could be a promising technique for studying 21cm images (Datta et al., 2007, 2008; Majumdar et al., 2011, 2012; Mishra et al., 2025). This method enhances the detection of ionised regions by convolving a filter, shaped to match the expected 21cm signal, with the observed visibilities. The signal-to-noise ratio (SNR) of this convolution is maximised when the filter closely matches the true 21cm signal (c.f. Fig. 7). By testing different spherical ionised region sizes, this approach effectively determines ionised region sizes and traces the IGM HI fraction.

Studies have explored filters mimicking a spherical ionised region within a uniform HI background, using toy models and semi-numerical simulations to assess the feasibility of measuring the ionised region sizes (or bubbles) around galaxies, in particular those hosting quasars, with SKA1-Low. For example, Mishra et al. (2025) found that with 100–200 hours of SKA1-Low observations, ionised regions larger than $\sim$ 20 cMpc around galaxies could be detected in a Universe that is up to 50% ionised. The combination of wide-area surveys for high-redshift Lyman-$\alpha$ emitters in regions of the sky suitable for SKA observations should, when followed-up with deep JWST spectroscopy (e.g. Lu et al. 2024; Nikolić et al. 2025), result in a sample of ionized bubbles suitable for size measurements based on 21cm observations. A key advantage of targeting ionised regions around already detected galaxies is that determining their sizes is primarily limited by the instrument's resolution. In contrast, blind searches may struggle to detect smaller ($<$ 10 cMpc) ionised regions.

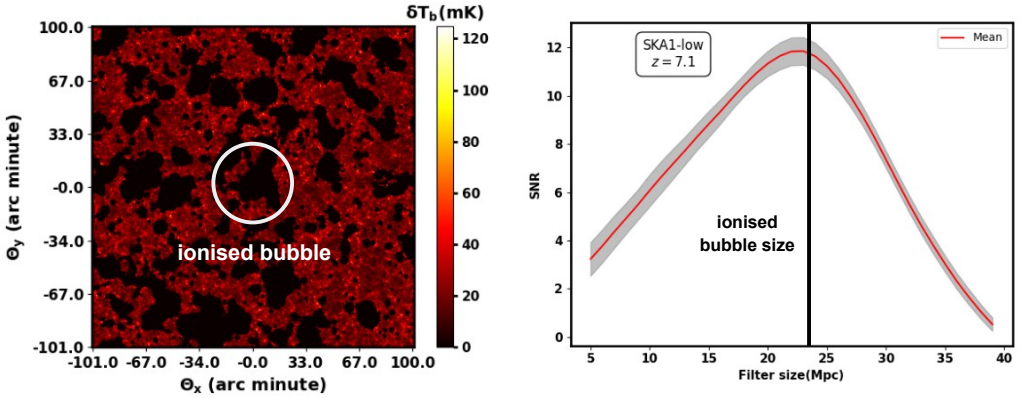


**Figure 7:** *Left:* 21cm differential brightness temperature distribution at $z = 7.1$ and $\langle \chi_{\rm HI} \rangle = 0.52$ centering on an ionised regions with a size of 23.5 cMpc (Mishra et al., 2025). *Right:* Signal-to-noise ratio from matched filtering applied to 20 independent noise realizations of 200 hours SKA1-Low observations (Mishra et al., 2025). The shaded region indicates the $1\sigma$ uncertainty from the realizations.

Since the 21cm signal amplitude around the ionised region is proportional to the mass-averaged HI fraction outside the ionised region, the SNR value can also be used to trace the IGM's mean HI fraction (Mishra et al., 2025). While promising, further work is needed to fully understand how ionised region detection and HI fraction constraints will behave during the early cosmic epochs, when the first ionised regions begin to form, the IGM HI fraction is high, and IGM heating is still ongoing. A different approach delineates ionised bubble boundaries in three dimensions, enabling robust inference of quasar lifetimes, ionizing luminosities, and IGM conditions. Bolgar et al. (2018) illustrated how variations in quasar duty cycles leave distinct signatures in 21 cm tomography, though detectability remains challenging.

### *4.1.2 Constraints from galaxy-informed stacking of 21cm fields*

A few studies have explored how stacking 21cm fields around pre-selected galaxies or empty regions can probe ionised region sizes, the global IGM ionisation state, and the reionisation morphology.

**Stacking 21cm images around galaxies** Sources detected by JWST, Roman, or Euclid will reveal average 21cm profiles for different galaxy samples, such as those grouped by ultraviolet (UV) luminosity. Davies et al. (2021) demonstrated that both the amplitude and width of these profiles increase with the size of ionised regions, with the latter reflecting the greater asymmetry of more spatially extended ionised regions. Additionally, the profile's sign indicates whether the 21cm signal is in emission or absorption, being negative (positive) when the spin temperature is saturated (unsaturated). Analyses of reionisation simulations reveal that in an ideal case without foreground contamination a $5\sigma$ detection at $z \sim 9$ is possible with images from 30 galaxies. However, in presence of foregrounds, only images around 100 of the brightest galaxies in the SKA1-Low FoV could yield a $1.4\sigma$ detection at $z \sim 9$; partial foreground removal can achieve detections with fewer images (see Fig. 8). By analysing the amplitudes and widths of average 21cm profiles around galaxies of varying UV luminosities, we can constrain the size distribution of ionised regions and the overall ionisation morphology (Wyithe et al., 2005; Geil et al., 2017; Davies et al., 2021). Broader,

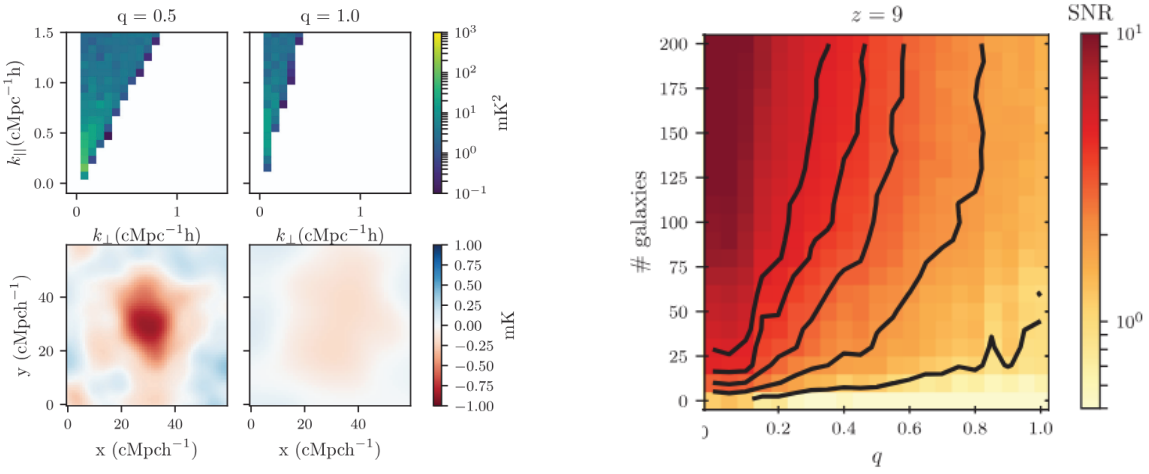


**Figure 8:** *Left:* Stacked simulated 21cm images of ionised regions around galaxies at $z = 9$ for two foreground models from Davies et al. (2021): maximal contamination ($q = 1$) and a reduced case where foreground subtraction halves the horizon slope ($q = 0.5$). Top panels show the stacked 21cm signal in cylindrically average Fourier space, and the bottom panels show slices of the centre of the stacked profiles. *Right:* Signal-to-noise ratio (SNR) for detecting the stacked ionized regions at $z = 9$ as a function of foreground level and number of galaxies. Contours from right to left correspond to SNR = (1, 2, 3, 4, 5).

shallower profiles around UV-bright galaxies –suggesting more asymmetric ionised regions (Hutter et al., 2023b) – may indicate reionisation scenarios driven by faint galaxies, though further validation is needed.

**Differences in the average 21cm differential brightness temperatures between regions with and without Lyman-alpha emitting galaxies (LAEs)** can constrain the IGM's ionisation state and reionisation morphology. Lyman-alpha radiation is sensitive to HI absorption. However galaxies are biased tracers of the matter field and so trace regions that are likely overionized/overheated compared to average regions. By measuring the difference between the average 21cm signal ($\Delta T^{(\mathrm{LAE})}$) on 1-5 arcmin scales in regions containing and lacking LAEs with 1000 hours SKA observations (V4A array configuration), we can learn about the ionization state and morphology of the IGM. For example, analysing 10 fields with and without LAEs, this method can differentiate an IGM 10% neutral from one that is 50% neutral (Hutter et al., 2017).The measured difference mimics the small-scale 21cm-LAE cross-correlation amplitude and inherits its dependencies on the ionisation morphology. As reionisation is driven more by fainter galaxies, the ionisation field becomes more strongly correlated with the underlying density field, reducing the 21cm signal

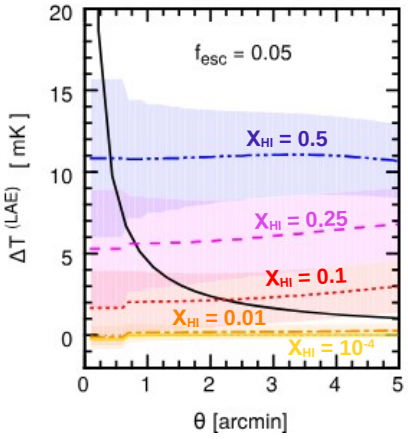


**Figure 9:** Difference in the 21cm signal between regions with and without LAEs, averaged over 10 fields, as a function of angular size for 1000 hours SKA observations (Hutter et al., 2017).

amplitude difference between LAE and non-LAE regions (Hutter et al., 2023b).

## 5 Conclusions

In this chapter we reviewed the current state of knowledge about the IGM and galaxies during the EoR. As we approach the first 21cm detection of the EoR with the SKA, synergies with other facilities will be essential both to verify its cosmological origin as well as to help mitigate unknown systematics. Therefore it is essential to plan SKA-low observations keeping in mind overlap with other surveys.

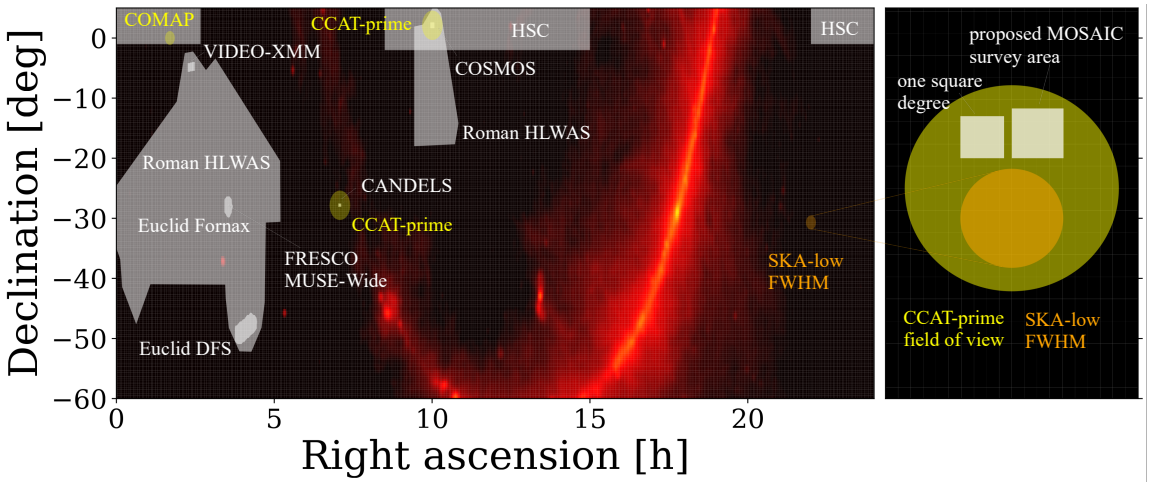


**Figure 10:** The southern sky from Declination −60 to the equator with overlaid galaxy surveys (white) and line intensity mapping surveys (yellow) which have already been carried out or will be carried out by 2030. The SKA-low FWHM is shown in orange for scale, with the right panel comparing the size of a proposed MOSAIC survey to pointings of the SKA-low and CCAT-prime (MOSAIC Mesinger et al. (2024); Gagnon-Hartman et al. (2025); CCAT-prime CCAT-Prime Collaboration et al. (2023)). The background image was generated using the Global Sky Model at 150 MHz (de Oliveira-Costa et al., 2008).

In Figure 10 we show a map of the southern sky with existing and planned high-$z$ galaxy surveys (VIDEO-XMM: Jarvis et al. (2013); Roman HLWAS-Medium: Zasowski et al. (2025); HSC: Aihara et al. (2018a); Euclid Fornax, Euclid DFS: Euclid Collaboration et al. (2025); FRESCO: Oesch et al. (2023); MUSE-Wide: Herenz et al. (2017); CANDELS: Grogin et al. (2011); COSMOS: Shuntov et al. (2025)) overlaid in white, and existing and planned line intensity mapping surveys (COMAP: Cleary et al. (2022); CCAT-prime: CCAT-Prime Collaboration et al. (2023)) in yellow. Note that the FRESCO and MUSE-Wide surveys are located in the GOODS-S field. The right panel compares the size of a proposed MOSAIC survey (Mesinger et al., 2024; Gagnon-Hartman et al., 2025) to pointings of the SKA-low and CCAT-prime. From this figure we see that some obvious targets for cross correlations, such as the Subaru fields and COSMOS fields, are close to zero degrees. This highlights the importance of being able to observe with SKA-low even at low latitudes. Preliminary SKA observations must insure an overlapping footprint with such complimentary surveys.

**Author contributions**

A. Mesinger coordinated the writing of this chapter, edited the scientific content, and was responsible

for the introduction. P. Dayal coordinated writing Sec. 2.1, and contributed to the science in other sections. S.K. Giri coordinated writing Sec. 2.2. T. R. Choudhury coordinated writing Sec. 4.1 and contributed to several other sections. B. Maity contributed to writing Sections 2.1, 2.2, and 2.3. Y. Qin coordinated writing Sec 2.3, and contributed to the scientific content of the other sections. A. Chakraborty contributed to the text in Sections 2.1 and 2.3. C. Heneka coordinated and led the writing of section 3.2. S. Gagnon-Hartman, K. Moriwaki, and S. Yoshuira provided commenting and feedback. A. Gorce coordinated and led the writing of section 3.1. C. S. Murmu, S. Majumdar, and C. Heneka wrote most of the text in Section 3.3 of the chapter. A. Hutter coordinated and wrote most of Sec. 4.1 and contributed to Sec. 3.2. K. Datta provided input to Sec. 4.1. E. Zackrisson provided input and contributed to writing Sec. 4.1. S. Gagnon-Hartman made Figure 10. The other co-authors and the chapter lead further modified it to fit it seamlessly within the chapter.

## References

A. Acharya et al. *Monthly Notices of the Royal Astronomical Society*, 534(1):L30–L34, Oct. 2024. doi: 10.1093/mnrasl/slae078.

N. J. Adams et al. *The Astrophysical Journal*, 965(2):169, Apr. 2024. doi: 10.3847/1538-4357/ad2a7b.

P. J. Adshead and S. R. Furlanetto. *Monthly Notices of the Royal Astronomical Society*, 384(1): 291–304, Feb. 2008. doi: 10.1111/j.1365-2966.2007.12681.x.

H. Aihara et al. *Publications of the Astronomical Society of Japan*, 70:S4, Jan. 2018a. doi: 10.1093/pasj/psx066.

H. Aihara et al. *Publications of the Astronomical Society of Japan*, 70:S8, Jan. 2018b. doi: 10.1093/pasj/psx081.

H. B. Akins et al. *arXiv e-prints*, art. arXiv:2406.10341, June 2024. doi: 10.48550/arXiv.2406.10341.

S. S. Ali, S. Bharadwaj, and J. N. Chengalur. *Monthly Notices of the Royal Astronomical Society*, 385(4):2166–2174, Apr. 2008. doi: 10.1111/j.1365-2966.2008.12984.x.

M. A. Alvarez, E. Komatsu, O. Doré, and P. R. Shapiro. *The Astrophysical Journal*, 647(2): 840–852, Aug. 2006. doi: 10.1086/504888.

H. Atek et al. *Nature*, 626(8001):975–978, Feb. 2024. doi: 10.1038/s41586-024-07043-6.

D. Austin et al. *arXiv e-prints*, art. arXiv:2404.10751, Apr. 2024. doi: 10.48550/arXiv.2404.10751.

E. Bañados et al. *Nature*, 553(7689):473–476, Jan. 2018. doi: 10.1038/nature25180.

S. Balu et al. *Monthly Notices of the Royal Astronomical Society*, 520(3):3368–3382, 2023.

A. Beane and A. Lidz. *The Astrophysical Journal*, 867(1):26, Nov. 2018. doi: 10.3847/1538-4357/aae388.

S. V. W. Beckwith et al. *The Astronomical Journal*, 132(5):1729–1755, Nov. 2006. doi: 10.1086/507302.

R. Begley et al. *arXiv e-prints*, art. arXiv:2410.10988, Oct. 2024. doi: 10.48550/arXiv.2410.10988.

M. Béthermin et al. *Astronomy & Astrophysics*, 667:A156, Nov. 2022. doi: 10.1051/0004-6361/202243888.

A. Bhagwat, B. Ciardi, E. Zackrisson, and J. Schaye. *Monthly Notices of the Royal Astronomical Society*, 517(2):2331–2342, 10 2022. ISSN 0035-8711. doi: 10.1093/mnras/stac2663. URL https://doi.org/10.1093/mnras/stac2663.

S. Bharadwaj and S. S. Ali. *Monthly Notices of the Royal Astronomical Society*, 356(4):1519–1528, Feb. 2005. doi: 10.1111/j.1365-2966.2004.08604.x.

F. Bianchini and M. Millea. *Physical Review D*, 107(4):043521, Feb. 2023. doi: 10.1103/PhysRevD.107.043521.

E. Boera, G. D. Becker, J. S. Bolton, and F. Nasir. *The Astrophysical Journal*, 872(1):101, 2019.

P. Bolan et al. *Monthly Notices of the Royal Astronomical Society*, 517(3):3263–3274, 2022.

F. Bolgar, E. Eames, C. Hottier, and B. Semelin. *Monthly Notices of the Royal Astronomical Society*, 478(4):5564–5578, Aug. 2018. doi: 10.1093/mnras/sty1293.

J. S. Bolton et al. *Monthly Notices of the Royal Astronomical Society*, 406(1):612–625, 2010.

J. S. Bolton et al. *Monthly Notices of the Royal Astronomical Society*, 419(4):2880–2892, 2012.

S. E. Bosman et al. *Monthly Notices of the Royal Astronomical Society*, 514(1):55–76, 2022.

R. J. Bouwens et al. *The Astrophysical Journal*, 803(1):34, Apr. 2015. doi: 10.1088/0004-637X/803/1/34.

R. J. Bouwens et al. *The Astrophysical Journal*, 830(2):67, Oct. 2016. doi: 10.3847/0004-637X/830/2/67.

D. Breitman et al. *Monthly Notices of the Royal Astronomical Society*, 527(4):9833–9852, Feb. 2024. doi: 10.1093/mnras/stad3849.

P. C. Breysse and M. Rahman. *Monthly Notices of the Royal Astronomical Society*, 468(1):741–750, June 2017. doi: 10.1093/mnras/stx451.

P. C. Breysse et al. *The Astrophysical Journal*, 933(2):188, July 2022. doi: 10.3847/1538-4357/ac63c9.

S. Bruton, Y.-H. Lin, C. Scarlata, and M. J. Hayes. *The Astrophysical Journal Letters*, 949(2):L40, 2023.

C. L. Carilli. *The Astrophysical Journal Letters*, 730(2):L30, Apr. 2011. doi: 10.1088/2041-8205/730/2/L30.

C. L. Carilli and F. Walter. *Annual Review of Astronomy and Astrophysics*, 51(1):105–161, Aug. 2013. doi: 10.1146/annurev-astro-082812-140953.

B. Casavecchia, U. Maio, C. Péroux, and B. Ciardi. *Astronomy & Astrophysics*, 693:A119, Jan. 2025. doi: 10.1051/0004-6361/202452282.

M. Castellano et al. *arXiv e-prints*, art. arXiv:2504.05893, Apr. 2025. doi: 10.48550/arXiv.2504.05893.

CCAT-Prime Collaboration et al. *The Astrophysical Journal Supplement Series*, 264(1):7, Jan. 2023. doi: 10.3847/1538-4365/ac9838.

A. Chakraborty and T. R. Choudhury. *Journal of Cosmology and Astroparticle Physics*, 2024(7): 078, July 2024. doi: 10.1088/1475-7516/2024/07/078.

A. Chakraborty and T. R. Choudhury. *arXiv e-prints*, art. arXiv:2503.07590, Mar. 2025. doi: 10.48550/arXiv.2503.07590.

T.-C. Chang et al. *Bulletin of The AAS*, 51(3):282, May 2019. doi: 10.48550/arXiv.1903.11744.

I. Chemerynska et al. *The Astrophysical Journal Letters*, 976(1):L15, Nov. 2024. doi: 10.3847/2041-8213/ad8dc9.

Y.-T. Cheng, T.-C. Chang, and J. J. Bock. *The Astrophysical Journal*, 901(2):142, Oct. 2020. doi: 10.3847/1538-4357/abb023.

T. R. Choudhury, S. Mukherjee, and S. Paul. *Monthly Notices of the Royal Astronomical Society*, 501(1):L7–L11, Jan. 2021. doi: 10.1093/mnrasl/slaa185.

D. T. Chung. *Journal of Cosmology and Astroparticle Physics*, 2023(12):024, Dec. 2023. doi: 10.1088/1475-7516/2023/12/024.

J. Clarke et al. *Astronomy & Astrophysics*, 689:A101, Sept. 2024. doi: 10.1051/0004-6361/202450300.

K. A. Cleary et al. *The Astrophysical Journal*, 933(2):182, July 2022. doi: 10.3847/1538-4357/ac63cc.

A. Cooray. *Physical Review D*, 70(6):063509, Sept. 2004. doi: 10.1103/PhysRevD.70.063509.

N. F. Cothard et al. *Journal of Low Temperature Physics*, 199(3-4):898–907, Jan. 2020. doi: 10.1007/s10909-019-02297-1.

B. P. Crill et al. In M. Lystrup and M. D. Perrin, editors, *Space Telescopes and Instrumentation 2020: Optical, Infrared, and Millimeter Wave*, volume 11443 of *Society of Photo-Optical Instrumentation Engineers (SPIE) Conference Series*, page 114430I, Dec. 2020. doi: 10.1117/12.2567224.

M. Cruise et al. *Nature Astronomy*, 9:36–44, Jan. 2025. doi: 10.1038/s41550-024-02416-3.

M. Curti et al. *Astronomy & Astrophysics*, 684:A75, Apr. 2024. doi: 10.1051/0004-6361/202346698.

E. Curtis-Lake et al. *Nature Astronomy*, 7(5):622–632, 2023.

K. K. Datta, S. Bharadwaj, and T. R. Choudhury. *Monthly Notices of the Royal Astronomical Society*, 382(2):809–818, Dec. 2007. doi: 10.1111/j.1365-2966.2007.12421.x.

K. K. Datta, S. Majumdar, S. Bharadwaj, and T. R. Choudhury. *Monthly Notices of the Royal Astronomical Society*, 391(4):1900–1912, Dec. 2008. doi: 10.1111/j.1365-2966.2008.14008.x.

F. B. Davies et al. *The Astrophysical Journal*, 864(2):142, Sept. 2018. doi: 10.3847/1538-4357/aad6dc.

J. E. Davies et al. *Monthly Notices of the Royal Astronomical Society*, 501(1):146–156, Feb. 2021. doi: 10.1093/mnras/staa3531.

P. Dayal. *Astronomy & Astrophysics*, 690:A182, Oct. 2024. doi: 10.1051/0004-6361/202451481.

P. Dayal and A. Ferrara. *Physics Reports*, 780:1–64, Dec. 2018. doi: 10.1016/j.physrep.2018.10.002.

P. Dayal et al. *Astronomy & Astrophysics*, 697:A211, May 2025. doi: 10.1051/0004-6361/202449331.

I. De Looze et al. *Astronomy & Astrophysics*, 568:A62, Aug. 2014. doi: 10.1051/0004-6361/201322489.

A. de Oliveira-Costa et al. *Monthly Notices of the Royal Astronomical Society*, 388(1):247–260, July 2008. doi: 10.1111/j.1365-2966.2008.13376.x.

D. R. DeBoer et al. , 129(974):045001, Apr. 2017. doi: 10.1088/1538-3873/129/974/045001.

J. Dhandha et al. *Monthly Notices of the Royal Astronomical Society*, 544(2):1608–1626, Dec. 2025a. doi: 10.1093/mnras/staf1736.

J. Dhandha et al. *Monthly Notices of the Royal Astronomical Society*, 542(3):2292–2322, Sept. 2025b. doi: 10.1093/mnras/staf1359.

T. Di Matteo, R. Perna, T. Abel, and M. J. Rees. *The Astrophysical Journal*, 564(2):576–580, Jan. 2002. doi: 10.1086/324293.

C. T. Donnan et al. *Monthly Notices of the Royal Astronomical Society*, 533(3):3222–3237, Sept. 2024. doi: 10.1093/mnras/stae2037.

O. Doré et al. *arXiv e-prints*, art. arXiv:1412.4872, Dec. 2014. doi: 10.48550/arXiv.1412.4872.

M. M. Dosibhatla et al. *arXiv e-prints*, art. arXiv:2508.09112, Aug. 2025. doi: 10.48550/arXiv.2508.09112.

S. Dumitru, G. Kulkarni, G. Lagache, and M. G. Haehnelt. *Monthly Notices of the Royal Astronomical Society*, 485(3):3486–3498, May 2019. doi: 10.1093/mnras/stz617.

C. Dvorkin and K. M. Smith. *Physical Review D*, 79(4):043003, Feb. 2009. doi: 10.1103/PhysRevD.79.043003.

Euclid Collaboration et al. *Astronomy & Astrophysics*, 697:A1, May 2025. doi: 10.1051/0004-6361/202450810.

C. Evoli, A. Mesinger, and A. Ferrara. *Journal of Cosmology and Astroparticle Physics*, 11:024, Nov. 2014. doi: 10.1088/1475-7516/2014/11/024.

G. Facchinetti, L. Lopez-Honorez, Y. Qin, and A. Mesinger. *Journal of Cosmology and Astroparticle Physics*, 2024(1):005, Jan. 2024. doi: 10.1088/1475-7516/2024/01/005.

X. Fan et al. *The Astronomical Journal*, 132(1):117, 2006.

E. R. Fernandez et al. *Monthly Notices of the Royal Astronomical Society*, 440(1):298–306, May 2014. doi: 10.1093/mnras/stu261.

T. Fragos et al. *The Astrophysical Journal*, 764:41, Feb. 2013. doi: 10.1088/0004-637X/764/1/41.

H. Fronenberg and A. Liu. *The Astrophysical Journal*, 975(2):222, Nov. 2024. doi: 10.3847/1538-4357/ad77cc.

S. R. Furlanetto, A. Sokasian, and L. Hernquist. *Monthly Notices of the Royal Astronomical Society*, 347(1):187–195, Jan. 2004. doi: 10.1111/j.1365-2966.2004.07187.x.

S. Gagnon-Hartman, J. Davies, and A. Mesinger. *arXiv e-prints*, art. arXiv:2502.20447, Feb. 2025.

P. Gaikwad et al. *Monthly Notices of the Royal Astronomical Society*, 494(4):5091–5109, 2020.

E. Garaldi et al. *Monthly Notices of the Royal Astronomical Society*, 512(4):4909–4933, 2022.

K. Gebhardt et al. *The Astrophysical Journal*, 923(2):217, Dec. 2021. doi: 10.3847/1538-4357/ac2e03.

P. M. Geil et al. *Monthly Notices of the Royal Astronomical Society*, 472(2):1324–1335, Dec. 2017. doi: 10.1093/mnras/stx1841.

T. Gessey-Jones et al. *arXiv e-prints*, art. arXiv:2304.07201, Apr. 2023. doi: 10.48550/arXiv.2304.07201.

R. Ghara et al. *Monthly Notices of the Royal Astronomical Society*, 503(3):4551–4562, May 2021. doi: 10.1093/mnras/stab776.

S. K. Giri et al. *Monthly Notices of the Royal Astronomical Society*, 533(2):2364–2378, 2024.

V. Gluscevic, M. Kamionkowski, and D. Hanson. *Physical Review D*, 87(4):047303, Feb. 2013. doi: 10.1103/PhysRevD.87.047303.

Y. Gong et al. *The Astrophysical Journal*, 745(1):49, Jan. 2012. doi: 10.1088/0004-637X/745/1/49.

A. Grazian et al. *The Astrophysical Journal*, 974(1):84, Oct. 2024. doi: 10.3847/1538-4357/ad6980.

J. E. Greene et al. *The Astrophysical Journal*, 964(1):39, Mar. 2024. doi: 10.3847/1538-4357/ad1e5f.

B. Greig and A. Mesinger. *Monthly Notices of the Royal Astronomical Society*, 449(4):4246–4263, June 2015. doi: 10.1093/mnras/stv571.

B. Greig, A. Mesinger, Z. Haiman, and R. A. Simcoe. *Monthly Notices of the Royal Astronomical Society*, 466(4):4239–4249, Apr. 2017. doi: 10.1093/mnras/stw3351.

B. Greig et al. *Monthly Notices of the Royal Astronomical Society*, 512(4):5390–5403, 2022.

N. A. Grogin et al. *The Astrophysical Journal Supplement Series*, 197(2):35, Dec. 2011. doi: 10.1088/0067-0049/197/2/35.

Y. Harikane et al. *The Astrophysical Journal*, 960(1):56, Jan. 2024. doi: 10.3847/1538-4357/ad0b7e.

T. Harvey et al. *The Astrophysical Journal*, 978(1):89, Jan. 2025. doi: 10.3847/1538-4357/ad8c29.

C. Heneka and A. Cooray. *Monthly Notices of the Royal Astronomical Society*, 506(2):1573–1584, Sept. 2021. doi: 10.1093/mnras/stab1842.

C. Heneka and A. Mesinger. *Monthly Notices of the Royal Astronomical Society*, 496(1):581–589, July 2020. doi: 10.1093/mnras/staa1517.

C. Heneka, A. Cooray, and C. Feng. *The Astrophysical Journal*, 848(1):52, Oct. 2017. doi: 10.3847/1538-4357/aa8eed.

HERA Collaboration et al. *The Astrophysical Journal*, 945(2):124, Mar. 2023. doi: 10.3847/1538-4357/acaf50.

E. C. Herenz et al. *Astronomy & Astrophysics*, 606:A12, Sept. 2017. doi: 10.1051/0004-6361/201731055.

G. P. Holder, I. T. Iliev, and G. Mellema. *The Astrophysical Journal Letters*, 663(1):L1–L4, July 2007. doi: 10.1086/519835.

T. Y.-Y. Hsiao et al. *The Astrophysical Journal*, 973(1):8, 2024.

J. Hunacek et al. *Journal of Low Temperature Physics*, 193(5-6):893–900, Dec. 2018. doi: 10.1007/s10909-018-1906-3.

A. Hutter, P. Dayal, V. Müller, and C. M. Trott. *The Astrophysical Journal*, 836(2):176, Feb. 2017. doi: 10.3847/1538-4357/836/2/176.

A. Hutter, C. M. Trott, and P. Dayal. *Monthly Notices of the Royal Astronomical Society*, 479(1): L129–L133, Sept. 2018. doi: 10.1093/mnrasl/sly115.

A. Hutter et al. *Monthly Notices of the Royal Astronomical Society*, 525(2):1664–1676, Oct. 2023a. doi: 10.1093/mnras/stad2376.

A. Hutter et al. *Monthly Notices of the Royal Astronomical Society*, 524(4):6124–6148, Oct. 2023b. doi: 10.1093/mnras/stad2230.

A. Hutter et al. *Astronomy & Astrophysics*, 694:A254, 2025.

A. K. Inoue et al. *Publications of the Astronomical Society of Japan*, 70(3):55, 2018.

D. Jain, T. R. Choudhury, S. Mukherjee, and S. Paul. *Monthly Notices of the Royal Astronomical Society*, 522(2):2901–2918, June 2023. doi: 10.1093/mnras/stad1149.

D. Jain, S. Mukherjee, and T. R. Choudhury. *Monthly Notices of the Royal Astronomical Society*, 527(2):2560–2572, Jan. 2024. doi: 10.1093/mnras/stad3277.

R. Jana and B. B. Nath. *Monthly Notices of the Royal Astronomical Society*, 479(1):153–161, Sept. 2018. doi: 10.1093/mnras/sty1481.

M. J. Jarvis et al. *Monthly Notices of the Royal Astronomical Society*, 428(2):1281–1295, Jan. 2013. doi: 10.1093/mnras/sts118.

V. Jelić et al. *Monthly Notices of the Royal Astronomical Society*, 402(4):2279–2290, Mar. 2010. doi: 10.1111/j.1365-2966.2009.16086.x.

X. Jin et al. *The Astrophysical Journal*, 942(2):59, 2023.

G. C. Jones et al. *Monthly Notices of the Royal Astronomical Society*, 536(3):2355–2380, 2025.

I. Jung et al. *The Astrophysical Journal*, 904(2):144, 2020.

Y. Kageura et al. *arXiv preprint arXiv:2501.05834*, 2025.

R. Kannan et al. *Monthly Notices of the Royal Astronomical Society*, 514(3):3857–3878, Aug. 2022. doi: 10.1093/mnras/stac1557.

C. Karoumpis et al. *Astronomy & Astrophysics*, 659:A12, Mar. 2022. doi: 10.1051/0004-6361/202141293.

C. Karoumpis et al. *Astronomy & Astrophysics*, 691:A262, Nov. 2024. doi: 10.1051/0004-6361/202450304.

O. Z. Katz, D. Redigolo, and T. Volansky. *Journal of Cosmology and Astroparticle Physics*, 2025 (10):047, Oct. 2025. doi: 10.1088/1475-7516/2025/10/047.

H. D. Kaur et al. *Monthly Notices of the Royal Astronomical Society*, 513(4):5097–5108, July 2022. doi: 10.1093/mnras/stac1226.

V. Kokorev et al. *The Astrophysical Journal*, 968(1):38, June 2024. doi: 10.3847/1538-4357/ad4265.

V. Kokorev et al. *The Astrophysical Journal Letters*, 983(1):L22, Apr. 2025. doi: 10.3847/2041-8213/adc458.

E. D. Kovetz et al. *arXiv e-prints*, art. arXiv:1709.09066, Sept. 2017. doi: 10.48550/arXiv.1709.09066.

K. Kubota et al. *Monthly Notices of the Royal Astronomical Society*, 479(2):2754–2766, Sept. 2018. doi: 10.1093/mnras/sty1471.

K. Kubota, A. K. Inoue, K. Hasegawa, and K. Takahashi. *Monthly Notices of the Royal Astronomical Society*, 494(3):3131–3140, May 2020. doi: 10.1093/mnras/staa979.

G. Kulkarni et al. *Monthly Notices of the Royal Astronomical Society: Letters*, 485(1):L24–L28, 2019.

K. E. Kunze. *Journal of Cosmology and Astroparticle Physics*, 2023(8):017, Aug. 2023. doi: 10.1088/1475-7516/2023/08/017.

P. La Plante, A. Lidz, J. Aguirre, and S. Kohn. *The Astrophysical Journal*, 899(1):40, Aug. 2020. doi: 10.3847/1538-4357/aba2ed.

G. Lagache, M. Cousin, and M. Chatzikos. *Astronomy & Astrophysics*, 609:A130, Jan. 2018. doi: 10.1051/0004-6361/201732019.

E. H. Lee et al. *Research Notes of the American Astronomical Society*, 9(4):96, Apr. 2025. doi: 10.3847/2515-5172/adcea7.

B. D. Lehmer et al. *The Astrophysical Journal Supplement Series*, 161(1):21–40, Nov. 2005. doi: 10.1086/444590.

N. Leite et al. *Monthly Notices of the Royal Astronomical Society*, 469(1):416–424, July 2017. doi: 10.1093/mnras/stx805.

T. K. D. Leung et al. *The Astrophysical Journal*, 905(2):102, Dec. 2020. doi: 10.3847/1538-4357/abc25e.

J. S. Lewis et al. *Monthly Notices of the Royal Astronomical Society*, 516(3):3389–3397, 2022.

J.-M. Liang, X.-C. Mao, and B. Qin. *Research in Astronomy and Astrophysics*, 16(8):132, Aug. 2016. doi: 10.1088/1674-4527/16/8/132.

L. Liang et al. *Monthly Notices of the Royal Astronomical Society*, 528(1):499–541, Feb. 2024. doi: 10.1093/mnras/stad3792.

A. Lidz et al. *The Astrophysical Journal*, 741(2):70, Nov. 2011. doi: 10.1088/0004-637X/741/2/70.

A. Liu and M. Tegmark. *Physical Review D*, 83(10):103006, May 2011. doi: 10.1103/PhysRevD.83.103006.

H. Liu and T. R. Slatyer. *Physical Review D*, 98(2):023501, July 2018. doi: 10.1103/PhysRevD.98.023501.

L.-J. Liu et al. *The Astrophysical Journal*, 974(2):175, Oct. 2024. doi: 10.3847/1538-4357/ad73d5.

M. Llerena et al. *arXiv e-prints*, art. arXiv:2412.01358, Dec. 2024. doi: 10.48550/arXiv.2412.01358.

L. Lopez-Honorez et al. *Journal of Cosmology and Astroparticle Physics*, 8:004, Aug. 2016. doi: 10.1088/1475-7516/2016/08/004.

T.-Y. Lu et al. *arXiv e-prints*, art. arXiv:2411.04176, Nov. 2024. doi: 10.48550/arXiv.2411.04176.

Q. Ma, B. Ciardi, M. B. Eide, and K. Helgason. *Monthly Notices of the Royal Astronomical Society*, 480(1):26–34, Oct. 2018a. doi: 10.1093/mnras/sty1806.

Q. Ma et al. *Monthly Notices of the Royal Astronomical Society*, 476(3):4025–4031, May 2018b. doi: 10.1093/mnras/sty543.

P. Madau. *The Astrophysical Journal*, 851(1):50, Dec. 2017. doi: 10.3847/1538-4357/aa9715.

P. Madau, E. Giallongo, A. Grazian, and F. Haardt. *The Astrophysical Journal*, 971(1):75, Aug. 2024. doi: 10.3847/1538-4357/ad5ce8.

R. Maiolino et al. *Astronomy & Astrophysics*, 691:A145, Nov. 2024. doi: 10.1051/0004-6361/202347640.

B. Maity and T. R. Choudhury. *Monthly Notices of the Royal Astronomical Society*, 511(2): 2239–2258, Apr. 2022a. doi: 10.1093/mnras/stac182.

B. Maity and T. R. Choudhury. *Monthly Notices of the Royal Astronomical Society*, 515(1):617–630, Sept. 2022b. doi: 10.1093/mnras/stac1847.

S. Majumdar, S. Bharadwaj, K. K. Datta, and T. R. Choudhury. *Monthly Notices of the Royal Astronomical Society*, 413(2):1409–1418, May 2011. doi: 10.1111/j.1365-2966.2011.18223.x.

S. Majumdar, S. Bharadwaj, and T. R. Choudhury. *Monthly Notices of the Royal Astronomical Society*, 426(4):3178–3194, Nov. 2012. doi: 10.1111/j.1365-2966.2012.21914.x.

X.-C. Mao. *The Astrophysical Journal*, 790(2):148, Aug. 2014. doi: 10.1088/0004-637X/790/2/148.

L. Mas-Ribas et al. *The Astrophysical Journal*, 950(1):39, June 2023. doi: 10.3847/1538-4357/acc9b2.

N. Mashian, A. Sternberg, and A. Loeb. *Journal of Cosmology and Astroparticle Physics*, 2015 (11):028–028, Nov. 2015. doi: 10.1088/1475-7516/2015/11/028.

C. A. Mason et al. *The Astrophysical Journal*, 856(1):2, 2018.

C. A. Mason et al. *Monthly Notices of the Royal Astronomical Society*, 485(3):3947–3969, 2019.

C. A. Mason et al. *arXiv preprint arXiv:2501.11702*, 2025.

J. Matthee et al. *The Astrophysical Journal*, 963(2):129, Mar. 2024. doi: 10.3847/1538-4357/ad2345.

I. D. McGreer, A. Mesinger, and V. D'Odorico. *Monthly Notices of the Royal Astronomical Society*, 447(1):499–505, 2015.

M. McQuinn et al. *The Astrophysical Journal*, 630(2):643–656, Sept. 2005. doi: 10.1086/432049.

M. McQuinn et al. *Monthly Notices of the Royal Astronomical Society*, 377:1043–1063, May 2007. doi: 10.1111/j.1365-2966.2007.11489.x.

P. D. Meerburg, C. Dvorkin, and D. N. Spergel. *The Astrophysical Journal*, 779(2):124, Dec. 2013. doi: 10.1088/0004-637X/779/2/124.

P. D. Meerburg, J. Meyers, K. M. Smith, and A. van Engelen. *Physical Review D*, 95(12):123538, June 2017. doi: 10.1103/PhysRevD.95.123538.

F. Mertens et al. *Astronomy & Astrophysics*, 698:A186, 2025.

A. Mesinger. *Monthly Notices of the Royal Astronomical Society*, 407(2):1328–1337, Sept. 2010. doi: 10.1111/j.1365-2966.2010.16995.x.

A. Mesinger, editor. *Understanding the Epoch of Cosmic Reionization*, volume 423 of *Astrophysics and Space Science Library*, Jan. 2016. doi: 10.1007/978-3-319-21957-8.

A. Mesinger. *The cosmic 21-cm revolution: charting the first billion years of our universe*. 2020. doi: 10.1088/2514-3433/ab4a73.

A. Mesinger, S. Furlanetto, and R. Cen. *Monthly Notices of the Royal Astronomical Society*, 411 (2):955–972, Feb. 2011. doi: 10.1111/j.1365-2966.2010.17731.x.

A. Mesinger, M. McQuinn, and D. N. Spergel. *Monthly Notices of the Royal Astronomical Society*, 422:1403–1417, May 2012. doi: 10.1111/j.1365-2966.2012.20713.x.

A. Mesinger, A. Ewall-Wice, and J. Hewitt. *Monthly Notices of the Royal Astronomical Society*, 439(4):3262–3274, Apr. 2014. doi: 10.1093/mnras/stu125.

A. Mesinger et al. *The Messenger*, 193:24–29, Sept. 2024. doi: 10.18727/0722-6691/5365.

J. Mirocha et al. *The Astrophysical Journal*, 983(1):54, Apr. 2025. doi: 10.3847/1538-4357/adbdce.

A. Mishra et al. *Journal of Cosmology and Astroparticle Physics*, 2025(2):055, Feb. 2025. doi: 10.1088/1475-7516/2025/02/055.

A. Moradinezhad Dizgah et al. *The Astrophysical Journal*, 926(2):137, Feb. 2022. doi: 10.3847/1538-4357/ac3edd.

A. M. Morales et al. *The Astrophysical Journal*, 919(2):120, 2021.

M. F. Morales, B. Hazelton, I. Sullivan, and A. Beardsley. *The Astrophysical Journal*, 752(2):137, June 2012. doi: 10.1088/0004-637X/752/2/137.

K. Moriwaki, N. Yoshida, M. B. Eide, and B. Ciardi. *Monthly Notices of the Royal Astronomical Society*, 489(2):2471–2477, Oct. 2019. doi: 10.1093/mnras/stz2308.

K. Moriwaki, A. Beane, and A. Lidz. *Monthly Notices of the Royal Astronomical Society*, 530(3): 3183–3194, May 2024. doi: 10.1093/mnras/stae1050.

S. Mukherjee, S. Paul, and T. R. Choudhury. *Monthly Notices of the Royal Astronomical Society*, 486(2):2042–2049, June 2019. doi: 10.1093/mnras/stz1002.

C. S. Murmu, S. Majumdar, and K. K. Datta. *Monthly Notices of the Royal Astronomical Society*, 507(2):2500–2509, Oct. 2021. doi: 10.1093/mnras/stab2347.

C. S. Murmu, R. Ghara, S. Majumdar, and K. K. Datta. *Journal of Astrophysics and Astronomy*, 43(2):104, Dec. 2022. doi: 10.1007/s12036-022-09882-z.

C. S. Murmu et al. *Monthly Notices of the Royal Astronomical Society*, 518(2):3074–3082, Jan. 2023. doi: 10.1093/mnras/stac3304.

S. Murray et al. *The Journal of Open Source Software*, 5(54):2582, Oct. 2020. doi: 10.21105/joss.02582.

M. Nakane et al. *The Astrophysical Journal*, 967(1):28, 2024.

I. Nikolić et al. *arXiv e-prints*, art. arXiv:2501.07980, Jan. 2025. doi: 10.48550/arXiv.2501.07980.

C. D. Nunhokee et al. *The Astrophysical Journal*, 989(1):57, Aug. 2025. doi: 10.3847/1538-4357/adda45.

P. A. Oesch et al. *The Astrophysical Journal*, 855(2):105, Mar. 2018. doi: 10.3847/1538-4357/aab03f.

P. A. Oesch et al. *Monthly Notices of the Royal Astronomical Society*, 525(2):2864–2874, Oct. 2023. doi: 10.1093/mnras/stad2411.

M. Ouchi et al. *Publications of the Astronomical Society of Japan*, 70(SP1):S13, 2018.

G. Paciga et al. *Monthly Notices of the Royal Astronomical Society*, 413(2):1174–1183, 04 2011. ISSN 0035-8711. doi: 10.1111/j.1365-2966.2011.18208.x. URL https://doi.org/10.1111/j.1365-2966.2011.18208.x.

H. Padmanabhan. *Monthly Notices of the Royal Astronomical Society*, 475(2):1477–1484, Apr. 2018. doi: 10.1093/mnras/stx3250.

H. Padmanabhan and A. Loeb. *arXiv e-prints*, art. arXiv:2408.16820, Aug. 2024. doi: 10.48550/arXiv.2408.16820.

H. Padmanabhan, P. Breysse, A. Lidz, and E. R. Switzer. *Monthly Notices of the Royal Astronomical Society*, 515(4):5813–5822, Oct. 2022. doi: 10.1093/mnras/stac2025.

S. Paul, S. Mukherjee, and T. R. Choudhury. *Monthly Notices of the Royal Astronomical Society*, 500(1):232–246, Jan. 2021. doi: 10.1093/mnras/staa3221.

Planck Collaboration et al. *Astronomy & Astrophysics*, 596:A108, Dec. 2016. doi: 10.1051/0004-6361/201628897.

A. R. Pullen, O. Doré, and J. Bock. *The Astrophysical Journal*, 786(2):111, May 2014. doi: 10.1088/0004-637X/786/2/111.

Y. Qin et al. *Monthly Notices of the Royal Astronomical Society*, 472(2):2009–2027, Dec. 2017. doi: 10.1093/mnras/stx1909.

Y. Qin et al. *Monthly Notices of the Royal Astronomical Society*, 499(1):550–558, Nov. 2020. doi: 10.1093/mnras/staa2797.

Y. Qin et al. *Publications of the Astronomical Society of Australia*, 42:e049, 2025.

C. L. Reichardt et al. *The Astrophysical Journal*, 908(2):199, Feb. 2021. doi: 10.3847/1538-4357/abd407.

P. Rinaldi et al. *The Astrophysical Journal*, 969(1):12, July 2024. doi: 10.3847/1538-4357/ad4147.

B. E. Robertson, R. S. Ellis, S. R. Furlanetto, and J. S. Dunlop. *The Astrophysical Journal Letters*, 802:L19, Apr. 2015.

A. Roy, A. Lapi, D. Spergel, and C. Baccigalupi. *Journal of Cosmology and Astroparticle Physics*, 2018(5):014, May 2018. doi: 10.1088/1475-7516/2018/05/014.

A. Roy et al. *Journal of Cosmology and Astroparticle Physics*, 2020(3):062, Mar. 2020. doi: 10.1088/1475-7516/2020/03/062.

A. Roy et al. *Journal of Cosmology and Astroparticle Physics*, 2021(1):003, Jan. 2021. doi: 10.1088/1475-7516/2021/01/003.

A. Roy et al. *The Astrophysical Journal*, 957(2):87, Nov. 2023. doi: 10.3847/1538-4357/acf92f.

A. Roy, A. Pullen, P. C. Breysse, and R. S. Somerville. *arXiv e-prints*, art. arXiv:2512.13943, Dec. 2025. doi: 10.48550/arXiv.2512.13943.

R. Salvaterra, B. Ciardi, A. Ferrara, and C. Baccigalupi. *Monthly Notices of the Royal Astronomical Society*, 360(3):1063–1068, July 2005. doi: 10.1111/j.1365-2966.2005.09089.x.

M. G. Santos, A. Cooray, and L. Knox. *The Astrophysical Journal*, 625(2):575–587, June 2005. doi: 10.1086/429857.

N. S. Sartorio et al. *Monthly Notices of the Royal Astronomical Society*, 521(3):4039–4055, May 2023. doi: 10.1093/mnras/stad697.

G. Sato-Polito, N. Kokron, and J. L. Bernal. *Monthly Notices of the Royal Astronomical Society*, 526(4):5883–5899, Dec. 2023. doi: 10.1093/mnras/stad2498.

S. Sazonov and R. Sunyaev. *Monthly Notices of the Royal Astronomical Society*, 454(4):3464–3471, Dec. 2015. doi: 10.1093/mnras/stv2255.

J. Schaye et al. *Monthly Notices of the Royal Astronomical Society*, 318(3):817–826, 2000.

J. Scholtz et al. *Astronomy & Astrophysics*, 697:A175, May 2025. doi: 10.1051/0004-6361/202348804.

T. Schutt et al. *Physical Review D*, 109(10):103539, May 2024. doi: 10.1103/PhysRevD.109.103539.

H.-Y. Shan and B. Qin. *Research in Astronomy and Astrophysics*, 9(1):73–84, Jan. 2009. doi: 10.1088/1674-4527/9/1/006.

M. Shuntov et al. *arXiv e-prints*, art. arXiv:2506.03243, June 2025. doi: 10.48550/arXiv.2506.03243.

B. M. Silva, S. Zaroubi, R. Kooistra, and A. Cooray. *Monthly Notices of the Royal Astronomical Society*, 475(2):1587–1608, Apr. 2018. doi: 10.1093/mnras/stx3265.

M. Silva, M. G. Santos, A. Cooray, and Y. Gong. *The Astrophysical Journal*, 806(2):209, June 2015. doi: 10.1088/0004-637X/806/2/209.

M. B. Silva et al. *The Astrophysical Journal*, 763(2):132, Feb. 2013. doi: 10.1088/0004-637X/763/2/132.

C. Simmonds et al. *Monthly Notices of the Royal Astronomical Society*, 535(4):2998–3019, Dec. 2024. doi: 10.1093/mnras/stae2537.

E. Sobacchi and A. Mesinger. *Monthly Notices of the Royal Astronomical Society*, 453(2):1843–1854, 2015.

E. Sobacchi, A. Mesinger, and B. Greig. *Monthly Notices of the Royal Astronomical Society*, 459 (3):2741–2750, July 2016. doi: 10.1093/mnras/stw811.

B. Spina et al. *Astronomy & Astrophysics*, 688:L26, 2024.

N. O. Stutzer et al. *Astronomy & Astrophysics*, 691:A336, Nov. 2024. doi: 10.1051/0004-6361/202451123.

G. Sun et al. *The Astrophysical Journal*, 915(1):33, July 2021a. doi: 10.3847/1538-4357/abfe62.

G. Sun, J. Mirocha, R. H. Mebane, and S. R. Furlanetto. *Monthly Notices of the Royal Astronomical Society*, 508(2):1954–1972, Dec. 2021b. doi: 10.1093/mnras/stab2697.

G. Sun et al. *The Astrophysical Journal*, 950(1):40, June 2023. doi: 10.3847/1538-4357/acc9b3.

G. Sun et al. *The Astrophysical Journal*, 981(1):92, Mar. 2025. doi: 10.3847/1538-4357/adae12.

M. Tang et al. *The Astrophysical Journal*, 972(1):56, 2024.

H. Tashiro et al. *Monthly Notices of the Royal Astronomical Society*, 389(1):469–477, Sept. 2008. doi: 10.1111/j.1365-2966.2008.13606.x.

H. Tashiro et al. *Monthly Notices of the Royal Astronomical Society*, 402(4):2617–2625, Mar. 2010. doi: 10.1111/j.1365-2966.2009.16078.x.

H. Tashiro et al. *Monthly Notices of the Royal Astronomical Society*, 414(4):3424–3433, July 2011. doi: 10.1111/j.1365-2966.2011.18644.x.

A. J. Taylor et al. *arXiv e-prints*, art. arXiv:2409.06772, Sept. 2024. doi: 10.48550/arXiv.2409.06772.

T. Theuns et al. *The Astrophysical Journal*, 567(2):L103, 2002.

C. M. Trott et al. Deep multi-redshift limits on Epoch of Reionisation 21 cm Power Spectra from Four Seasons of Murchison Widefield Array Observations. Technical report, 2020. URL http://skatelescope.org.

H. Umeda et al. *The Astrophysical Journal*, 971(2):124, 2024.

H. Umeda et al. *The Astrophysical Journal Supplement Series*, 277(2):37, 2025.

M. Van Cuyck et al. *Astronomy & Astrophysics*, 676:A62, Aug. 2023. doi: 10.1051/0004-6361/202346270.

H. Vedantham, N. Udaya Shankar, and R. Subrahmanyan. *The Astrophysical Journal*, 745(2):176, Feb. 2012. doi: 10.1088/0004-637X/745/2/176.

E. Visbal and M. McQuinn. *The Astrophysical Journal Letters*, 863(1):L6, Aug. 2018. doi: 10.3847/2041-8213/aad5e6.

D. Vrbanec et al. *Monthly Notices of the Royal Astronomical Society*, 492(4):4952–4958, Mar. 2020. doi: 10.1093/mnras/staa183.

M. Walther, J. Oñorbe, J. F. Hennawi, and Z. Lukić. *The Astrophysical Journal*, 872(1):13, 2019.

J. R. Weaver et al. *The Astrophysical Journal Supplement Series*, 258(1):11, Jan. 2022. doi: 10.3847/1538-4365/ac3078.

A. Weibel et al. *Monthly Notices of the Royal Astronomical Society*, 533(2):1808–1838, Sept. 2024. doi: 10.1093/mnras/stae1891.

L. Whitler et al. *arXiv e-prints*, art. arXiv:2501.00984, Jan. 2025. doi: 10.48550/arXiv.2501.00984.

I. G. Wold et al. *The Astrophysical Journal*, 927(1):36, 2022.

J. S. B. Wyithe, A. Loeb, and D. G. Barnes. *The Astrophysical Journal*, 634(2):715–727, Nov. 2005. doi: 10.1086/497160.

J. Yang et al. *The Astrophysical Journal*, 904(1):26, 2020.

S. Yang et al. *The Astrophysical Journal*, 929(2):140, Apr. 2022. doi: 10.3847/1538-4357/ac5d57.

S. Yoshiura et al. *Monthly Notices of the Royal Astronomical Society*, 479(2):2767–2776, Sept. 2018. doi: 10.1093/mnras/sty1472.

S. Yoshiura et al. *Monthly Notices of the Royal Astronomical Society*, 483(2):2697–2711, Feb. 2019. doi: 10.1093/mnras/sty3248.

S. Yoshiura et al. *MNRAS*, 000:1–15, 2021. URL https://lambda.gsfc.nasa.gov/product/foreground/fg_.

B. Yue and A. Ferrara. *Monthly Notices of the Royal Astronomical Society*, 490(2):1928–1943, Dec. 2019. doi: 10.1093/mnras/stz2728.

B. Yue et al. *Monthly Notices of the Royal Astronomical Society*, 450(4):3829–3839, July 2015. doi: 10.1093/mnras/stv933.

G. Zasowski et al. *arXiv e-prints*, art. arXiv:2505.10574, May 2025. doi: 10.48550/arXiv.2505.10574.

S. Zhang et al. *arXiv e-prints*, art. arXiv:2503.17585, Mar. 2025. doi: 10.48550/arXiv.2503.17585.

M. Zhou et al. *arXiv e-prints*, art. arXiv:2503.09462, Mar. 2025. doi: 10.48550/arXiv.2503.09462.

Y. Zhu et al. *The Astrophysical Journal*, 923(2):223, Dec. 2021. doi: 10.3847/1538-4357/ac26c2.

Y. Zhu et al. *Monthly Notices of the Royal Astronomical Society: Letters*, 533(1):L49–L56, 2024.